Design and Implementation of a 200 to 1600 MHz, Stepped Frequency, Ground Penetrating Radar Transceiver

Gordon Farquharson

A dissertation submitted to the Department of Electrical Engineering, University of Cape Town, in fulfilment of the requirements for the degree of Master of Science in Engineering.

Cape Town, August 1999

Declaration

I declare that this dissertation is my own, unaided work. It is being submitted for the degree of Master of Science in Engineering in the University of Cape Town. It has not been submitted before for any degree or examination in any other university.

Signature of Author .....

Cape Town
20 August 1999

Abstract

This thesis project deals with the design and construction of a 200 to 1600MHz, stepped frequency, ground penetrating radar transceiver. This dissertation describes the system specifications of the radar, the design procedure used, the implementation of the radar transceiver, and measurements made to determine the performance of the transceiver.

The dissertation briefly outlines the current state of ground penetrating radar technology. The system specifications of the transceiver are then developed and these are used to design the radar transceiver. The design considers various transceiver architectures, the synthesizer implementation using phase locked loops, and modification to the architecture for system phase coherence. The implementation of each of the transceiver modules is described showing specifications and specific designs for each. Laboratory measurements are made to measure the performance parameters of the transceiver and these are compared with the system specifications. The dissertation concludes with a summary of the work presented, a discussion on the performance of the radar with respect to the design and recommendations for the transceiver use and for future improvements.

The major results and conclusions of the thesis are that a stepped frequency, ground penetrating radar transceiver module was designed and constructed and found to operate with the radar but that there was an insufficient accuracy in phase noise measurements to characterise the causes for the transceiver limitations completely. There were also unexplained spurious harmonics close to the carrier signal at high frequencies. Despite these limitations, most of the system specifications were achieved with the exception of the dynamic range and synthesizer phase noise and the transceiver dynamic range performance can be improved by limiting the frequency band to less than 800MHz.

It was recommended that accurate measurements of the phase noise be made and that the IF harmonic levels be investigated to ensure that they do not significantly affect the radar data. It was also stated that the radar be used over a reduced bandwidth to improve the dynamic range.

Acknowledgements

The work presented in this dissertation for the degree of Master of Science was carried out as part of the Radar Remote Sensing Group's Ground Penetrating Radar Project at the University of Cape Town. This work was originally started with the financial assistance of Reunert, South Africa and completed with funding made available by Ball Aerospace, USA. For this funding and technical assistance received from each of these institutions, the author is especially grateful.

I would like to thank Professor M.R. Inggs for the opportunity to work in the UCT Remote Sensing Radar Group and Alan Langman for his supervision, ideas and motivation in this project.

I wish to thank Mr Steven Schrire and Mr Paul Daniels and for their technical assistance over the years.

A special thanks goes to my mother. Without her support throughout my life and especially during this project. all would have been so much more difficult.

Contents

List of Figures

List of Tables

List of Symbols

B	—	Transmitted RF bandwidth
c	—	Speed of light
f_c	—	Carrier frequency
f_i	—	Instantaneous frequency in stepped frequency sweep
f_{if}	—	IF frequency
f_n	—	Final transmitted frequency in stepped frequency sweep
f_0	—	Start frequency of stepped frequency sweep
F	—	Noise figure
G_r	—	Receive antenna gain
G_t	—	Transmit antenna gain
k	—	Boltzmann's constant
k	—	Propagation constant
P_r	—	Receive power
P_t	—	Transmit power
R	—	Range to target
$S_n(f)$	—	noise power spectral density
T_0	—	Operating temperature (298.15K)
v	—	Velocity of electromagnetic wave in a medium
α	—	Attenuation constant
β	—	Phase constant
δR	—	Range resolution
δx	—	Azimuth resolution
Δf	—	Frequency step size
ε	—	Permittivity
ε_0	—	Permittivity of free space
ε_r	—	Relative permittivity
θ	—	Instantaneous phase
λ	—	Wavelength
μ	—	Permeability
μ_0	—	Permeability of free space
μ_r	—	Relative permeability
σ	—	Conductivity

σ	—	Radar cross section
ω	—	Angular frequency

Nomenclature

Azimuth Angle in a horizontal plane, relative to a fixed reference, usually the longitudinal reference axis of the direction of motion of the radar.

Beamwidth The angular width of a slice through the mainlobe of the radiation pattern of an antenna in the horizontal, vertical or other plane. Usually taken between the 3dB points of the gain pattern.

CPLD Complex Logic Programmable Device.

DAC Digital to Analogue Convertor.

Doppler frequency A shift in the radio frequency of the return from a target or other object as a result of the object's radial motion relative to the radar.

FFT Fast Fourier Transform.

FPGA Field Programmable Gate Array.

GPR Ground Penetrating Radar. A device using electromagnetic techniques, designed for the detection of objects or interfaces beneath the earth's surface.

IF Intermediate Frequency. Refers to the center frequency of a frequency down-converted received radar signal.

RCS Radar Cross Section.

Single Sideband Phase Noise The sideband noise level in a 1Hz bandwidth, a specified distance from the center of the carrier, measured in rms Hz or dB relative to the carrier.

PLL Phase Locked Loop.

PRF Pulse Repetition Frequency.

SFCW Stepped Frequency Continuous Wave.

SRP Synthetic Range Profile.

Swath The area on earth covered by the antenna signal.

Synthetic Aperture Radar (SAR) A signal-processing technique for improving the azimuth resolution beyond the beamwidth of the physical antenna actually used in the radar system. This is done by synthesizing the equivalent of a very long sidelooking array antenna.

VCO Voltage Controlled Oscillator.

VHDL VHSIC (Very High Speed Integrated Circuit) Hardware Description Language.

Chapter 1

Introduction

This dissertation describes the design and implementation of a stepped frequency, continuous wave, ground penetrating radar transceiver. The transceiver was designed for the Mercury B system, being developed by the Radar Remote Sensing Group at the University of Cape Town. The transceiver was required to be portable, low cost and meet the system specifications presented in this document. The objectives of the thesis were to investigate and predict the performance of the transceiver and form a system specification; design and manufacture the transceiver; compare the specification with results obtained from radar measurements; and finally to draw conclusions.

1.1 Thesis Outline

This thesis document is organized as follows. The remainder of this chapter presents a brief summary of the current state of ground penetrating radar technology. This is followed by a presentation of the literature reviewed in completing this dissertation. From this theory, a simple simulation of the stepped frequency process was created and the results are presented. Chapter 2 develops the system specifications for the radar. A radar design is then presented in Chapter 3. This is achieved though a discussion on the architecture of the transceiver and the synthesizer design, where several architecture options are evaluated and solutions to problems inherent in the chosen architecture are presented. Chapter 4 describes the implementation of the radar. This description includes both the work done for this dissertation in the form of the transceiver module, and brief descriptions of the other modules, namely, the radar controller/data capture module and the power supply unit. The PC software is also briefly mentioned. Chapter 5

- **EMRAD** Pipehawk Ground Probing Radar System locates underground pipes and cables made of any material. It operates in real time, for emergencies and site mark-out, and instantly stores the data to provide plans in CAD format if required. The system operates from 100MHz to 1GHz with a wide band pulsed waveform. It has an average power transmission of 2mW. The pulse repetition frequency or peak pulse power are not specified.

  `http://www.emrad.com`

- **ENSCO** Proprietary GPR system is used to detect and locate underground voids at nuclear test facilities and has been used to detect and characterize waste burial trenches at the Rocky Mountain Arsenal near Denver, Colorado where the contents are unknown but could contain unexploded ordinance and other potentially hazardous debris.

  `http://www.ensco.com/Projects/gpr.htm`

- **Geophysical Survey Systems Inc. (GSSI)** Produces SIR-3, SIR-8, SIR System-2M, SIR System-2000, SIR System-2, SIR System-10B and SIR System-10H subsurface radars. Many different frequency configurations are available and customizable to the user's specific needs.

  `http://www.geophysical.com`

- **GeoRadar, Inc.** Manufactures a stepped-FM ground penetrating radar system.

  `http://www.georadar.com`

- **Ingegneria Dei Sistemi S.p.A. (IDS)** Manufactures propriety systems that are configurable to the user's needs.

  `http://www.ids-spa.it/`

- **MALA GeoScience** RAMAC/GPR system produced in 1994. The system is a derivative of the RAMAC borehole radar system in the early 1980's. Antennas for frequencies from 10MHz to 1000MHz are available. The radar has a 100kHz pulse repetition frequency and selectable number of samples per trace and stacking level.

  `http://www.malags.se`

- **Radar Systems Inc.** Products include the Zond-12c, Zond-14 and Python-02 radars. These radars have the electronics and batteries mounted inside the antenna structure.

  `http://www.radsys.lv/`

- **Road Radar LTD** The ROAD RADAR(TM) system has been developed specifically to non-destructively obtain subsurface information on roads and bridge decks. This systems resides in a van.

`http://www.rrl.com/home.html`

- **Sensors and Software** pulseEKKO and Noggin systems are the two product lines manufactured by Sensors and Software. The systems include the pulseEKKO 1000 with antenna frequencies of 110, 225, 900, 1200 MHz for high resolution mapping, the pulseEKKO 100 with antenna frequencies of 12.5, 25, 50, 100 and 200 for deep mapping, the Noggin 25 with a penetrating depth of up to 15 meters and the Noggin 500 with a penetration depth of up to 8 meters. These systems use pulse technology.

  `http://www.sensoft.on.ca/`

The state of the technology is most prominently reflected by the research institutions. A list is presented with a brief description of the current research.

- **Coleman Research Corporation (CRC)** Earth Penetration Radar Imaging System (EPRIS) is a stepped frequency system has been used by the Department of Defense (DOD), Department of Energy (DoE), and for archaeological surveys. EPRIS is a stepped frequency coherent system operating from 80-1000MHz [32].

- **Cooperative Research Centre for Sensor Signal and Information (CSSIP)** Two stepped-frequency GPR prototypes have been built. A 1-2GHz prototype has been developed and tested for high-resolution mapping of thin coal seam structures in open-cut coal mines [21]. The system has a maximum penetration depth of around 1 meter in coal, with a resolution of around 5 centimeters. A 10-620MHz [20] prototype is currently being developed and will be tested for mining applications which require a maximum penetration depth of between 10-20 meters in coal with coarser resolution.

  `http://www.cssip.elec.uq.edu.au/`

- **Demining Technology Center (DeTeC) at the EPFL** (November 1995 - December 1997) DeTeC worked on a sensor suite for Antipersonnel Mine Detection and actively supported (and still continues as far a possible) the exchange of information on demining technologies.

  `http://diwww.epfl.ch/w3lami/detec/detec.html`

- **Department of Energy, Special Technologies Laboratory** This system was originally designed to help the Navy find unexploded ordnance such as artillery shells. It has also been used to detected hazardous waste containers, underground utility pipes, tunnels, fossilized

dinosaur bones, as well as animal burrows. It is based on a frequency modulated-continuous wave (FM-CW) technique.

`http://www.nv.doe.gov/business/capabilities/fieldableproto/gndpenradar.htm`

- **ElectroScience Laboratory, Ohio State University** The ElectroScience Laboratory at the Ohio State University has been active in Ground Penetrating Radar research since the 1960's. The focus is currently on detecting and identifying anti-personnel mines and unexploded ordnance. Research is also being carried out in producing three dimensional images from GPR data and developing side-looking underground radar (SLUR) [8].

  `http://brewster.eng.ohio-state.edu/public_html/gpr.html`

- **International Research Centre for Telecommunications Transmission and Radar** IRCTR is involved in the antenna technology aspects of GPR [31]. The work involves enhancing the penetration of the GPR waves into the ground and the development of adaptive GPR antennas.

  `http://irctr.et.tudelft.nl/`

- **Radar Remote Sensing Group, University of Cape Town** The University of Cape Town started stepped frequency GPR research in 1990 with the use of a network analyser. In 1996, the first portable system had been constructed [16]. Since then, two systems have been produced.

  `http://rrsg.ee.uct.ac.za/~alan/minerad.htm`

- **University of Montana, Montana Tech** GPR research has been conducted at Montana Tech for several years. Recent and ongoing projects include void detection with particular interest in those underground cavities associated with past mining activities, studies of alluvial fan complexes on piedmont slopes of the Blue Ridge province, North Carolina and the development and use of 2-D and 3-D geophysical diffraction tomography algorithms for GPR data processing.

  `http://markov.mtech.edu/radar.html`

Chapter 2

System Specification

This chapter develops the system specification for the Mercury B stepped frequency, ground penetrating radar. The system specification sets the standard to which the final system design is required to perform. It is usually an ideal for the optimum performance of the system, given reasonable estimates of the materials from which the system will be constructed and environment in which the system will function. It acts as a starting point in the design of the system, towards which the engineer works.

Some of the specifications were estimated though experience with the previous Mercury GPR and others from calculations and simulations presented in this section. For a review of the concepts used in this section and an overview of stepped frequency radar and ground penetrating radar, refer to Appendix A.

2.1 Radar Specifications

2.1.1 Penetration Depth

Minimum Penetration Depth 0.5m

The penetration depth is difficult to calculate accurately as it is a complex function of the ground characteristics. However some estimates can be obtained from simple receiver and ground models. The models used for predictions are presented here.

The signal to noise ratio of a radar system determines the maximum penetration depth and can be determined from an evaluation of the radar equation,

modified appropriately for ground penetrating radar. The radar equation relates parameters inherent to the the radar, target and medium to the signal to noise ratio for a specified penetration depth.

The standard radar equation [37] must be modified for ground penetrating radar to take into account the attenuation caused by the ground, given by $e^{-4\alpha R}$. The received power, assuming far field antenna pattern, P_r, is then given by

$$P_r = \frac{P_t G_t G_r \lambda^2 \sigma e^{-4\alpha R}}{(4\pi)^3 R^4} \ [W] \tag{2.1}$$

where P_t is the transmitted power; G_t, the transmitter antenna gain; G_r, the receiver antenna gain; λ, the wavelength in the ground; σ, the radar cross section of the target; α, the attenuation coefficient of the medium; and R, the range to the target. The radar cross section, σ, in this case is calculated from the permittivity change between and the surrounding medium and the target as shown by Noon [21].

The minimum detectable signal at the receiver is determined by the receiver noise power spectral density, $S_n(f)$. Assuming a white noise model within the bandwidth of the receiver, any signal with a power spectral density maximum, less than the power spectral density of the noise floor of the receiver will be undetectable. The receiver noise power spectral density is given by

$$S_n(f) = kT_0F \ [\text{W/Hz}] \tag{2.2}$$

Assuming a synthesizer with no frequency drift, the received power will be concentrated to a single frequency. Therefore the signal power spectral density will be equal to the received power, P_r. For a single frequency, the maximum detection range will be the range at which signal power spectral density is equal to the noise power spectral density. The ratio of signal power spectral density to noise power spectral density will be referred to as the power spectral density signal to noise ratio, $(S/N)_{psd}$, and is given by

$$\left(\frac{S}{N}\right)_{psd} = \frac{P_t G_t G_r \lambda^2 \sigma e^{-4\alpha R}}{(4\pi)^3 kT_0 F L_s R^4} \tag{2.3}$$

where the factor L_s is included to account for any system loses, such as receiver losses and processing losses, and P_t is the power transmitted for one frequency step.

The noise power in the received signal will therefore be the integrated noise spectral density within the receiver bandwidth. Thus the minimum detectable signal is given by

$$P_{MDS} = kT_0FB_r \ [\text{W}] \tag{2.4}$$

where B_r is the receiver instantaneous bandwidth. The signal to noise ratio of the radar will then be

$$\frac{S}{N} = \frac{P_t G_t G_r \lambda^2 \sigma e^{-4\alpha R}}{(4\pi)^3 k T_0 F B_r L_s R^4} \tag{2.5}$$

The received signal is sampled and data is then coherently integrated to form the approximate synthetic range profile by the IDFT as shown in Appendix A. It is shown in [37] that for a point target the processing gain of this coherent integration is n if the target range is a multiple of the range resolution. This improves the power spectral density signal to noise ratio of the radar by $\sqrt{n}$. From Equation 2.5 we obtain Figure 2.1 which shows the signal to noise ratio from buried targets in different attenuation constants. The permittivity of the ground and the target were taken as $\varepsilon_{r(g)} = 5$ and $\varepsilon_{r(t)} = 1$ respectively, and a spherical target was assumed. The radar cross section was thus $2.58 \times 10^4 \mathrm{m}^2$ [21]. 140 frequency steps were used over a bandwidth of 200-1590MHz and the receiver bandwidth and noise figure were 100kHz and 3dB respectively. The antennas had a omnidirectional radiation pattern.

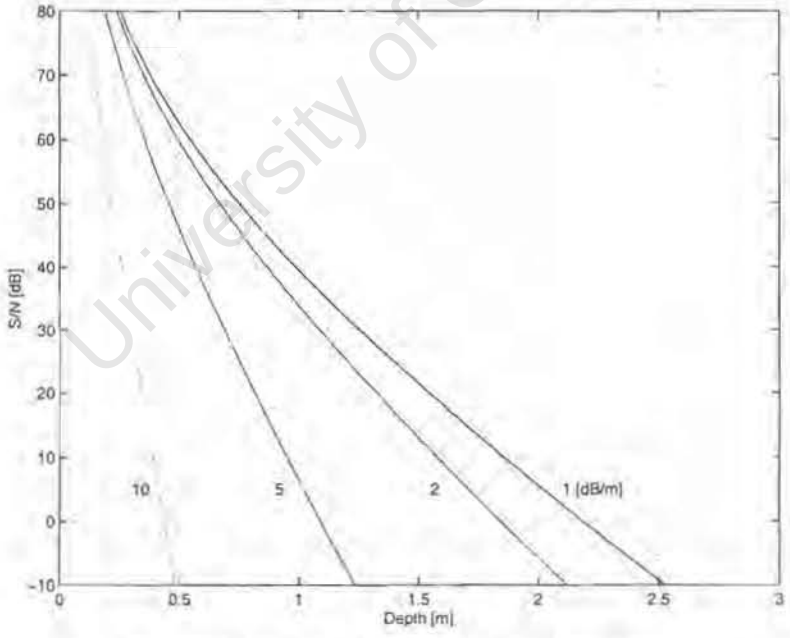

Figure 2.1: Signal to Noise Ratio vs Depth

The system specification requires that the minimum penetration depth be 0.5m. Figure 2.1 shows that this is possible in mediums with an attenuation constant less than 10dB/m.

2.1.2 Dynamic Range

Dynamic Range ..... > 70dB

The dynamic range is defined as the ratio of the maximum receiver power to the minimum detectable power within the bandwidth of the receiver. The maximum receiver power is the maximum power level that the components of the receiver system can handle before distorting the signal. This is determined by the 1dB compression point of the receiver. The minimum detectable power at the receiver is given by Equation 2.2 of the previous section. This is reduced by the coherent integration factor, n, as shown in the previous section.

In an ideal situation, the receiver dynamic range specifies the number of bits required by the radar sampling system. A 12 bit analogue to digital converter can achieve a theoretical 65dB signal to noise ratio (SNR), a 14 bit, 77dB SNR and a 16 bit, 89dB SNR. If the receiver dynamic range is greater than that of the ADC, then the required dynamic range will determine the requirements of the analogue to digital converter. As the system specification requires a 70dB dynamic range, the ADC will have to be 13 bits or more.

Dynamic range can also be limited by phase noise, spurious signals and harmonics. The phase noise specification is developed in Section 2.2.5. Examples of the latter include intermodulation products, reference frequency spurs, and the spurious free dynamic range of the ADC as supplied by the manufacturer. If these exceed the minimum detectable power level, they will appear as false targets in the synthetic range profile which can mask real targets, thus reducing the effective dynamic range.

For a receiver with a noise figure of 3dB and a 100kHz bandwidth at 290K, the minimum detectable signal from Equation 2.4 is -151dBm. If the maximum input power is -25dBm, then the dynamic range of the receiver is -126dBm. The actual dynamic range of the system will therefore be limited by the ADC quantization error or spurious signals.

2.1.3 Scan Speed

Number of Scans per Second 10

The specification was estimated using a reasonable value of 1m/s for the speed of the radar. For this speed, to achieve a scan every 10cm in azimuth, the number of scans per second is required to be 10.

2.1.4 Power Supply

Battery Supply Voltage Range ..... 9V to 18V

Maximum Current Consumption 2A

The radar is required to run from a 12V battery for several hours. The battery obtained for the Mercury B project is a 12V battery with a 2Ah current rating. Therefore, for 1 hour of operation, the radar is required to draw less than 2A.

The radar must also able to be run from an external battery. Therefore, the input voltage specification must be flexible to suit different voltages.

2.1.5 Temperature

Operating Temperature ..... 0°C to 60°C

Storage Temperature ..... −20°C to 70°C

To limit the cost of the radar, commercial grade components will be used. The operating and storage temperatures are therefore limited by the specifications of these components.

2.2 Transceiver Specifications

2.2.1 Frequency Range

Frequency Range ..... 200MHz - 1598MHz

The radar is to be capable of operating from 200MHz to 1598MHz in steps of 2MHz. This specification was chosen in conjunction with Ball Aerospace, one of the sponsors of the work done for the project, as it suited the requirements for their application. The radar, however, is capable of operating over any bandwidth in this frequency range, as configurable by the user. This feature is present as specific measurements might not require the full bandwidth of the radar or it might not be suitable to operate the radar over of the full frequency range. For example, the radar antennas might not cover the full transceiver range. The data capture procedure would therefore be faster

if the transceiver only operated over the antenna bandwidth, as the radar would not have to transmit the frequencies outside the antenna bandwidth.

The choice of frequency range depends on the ground characteristics, and, in part, the range resolution that is required to detect the targets. The ground parameters are obviously application dependent and are further discussed in Appendix A. The frequency range chosen was believed to be suitable for the applications of Ball Aerospace and is also adjustable for different measurement environments.

2.2.2 Frequency Step Size

Minimum Frequency Step Size 2MHz

The minimum radar frequency step size will be 2MHz. This minimum frequency step size is required as the the transmit and local oscillator synthesizer frequencies are required to be separated by the IF frequency (2MHz). As the synthesizers are identical in design, they are required to have this step size of 2MHz so that the LO synthesizer can output a frequency that is 2MHz higher than that of the TX synthesizer to generate the intermediate frequency.

A minimum step size of 2MHz also has the advantage that the number of frequency steps is user configurable in multiples of 2MHz. This is especially useful over reduced operating frequency ranges to achieve required range resolutions as the range resolution is inversely proportional to the number of frequency steps.

2.2.3 Number of Frequency Steps

Maximum 700

Default 140

The number of frequency steps, N, determines the unambiguous range of the radar and the number of scan per second achievable. This parameter is configurable by the user. The default value is used in this document to calculate any radar specifications dependent on N.

2.2.4 Harmonic Levels

Undesirable frequency harmonics will be present throughout the radar. However, at many points, these will not affect the performance of the radar. For instance, at the output of the synthesizers, the harmonic levels do not affect the radar's performance, as shown shown in Section 3.1. The two areas where the harmonic levels are important are now discussed.

Harmonics (inside IF bandwidth) ..... < -80dBc

Harmonic levels inside the IF bandwidth, at the output of the IF chain will corrupt the phase of the IF signal, and thus the distance to targets, as recorded by the radar. The levels inside the IF bandwidth should be less than that of the dynamic range of the receiver. They were thus chosen to be 10dB below the specified dynamic range parameter, or -80dBc.

Harmonics (outside IF bandwidth) ..... < -3dBc

Harmonic levels transmitted outside the band of radar operation are not desirable, as they will interfere with other electronic equipment in the vicinity but will not affect the performance of the radar. Government electromagnetic specifications impose limits on these levels. These limits were not adhered to in this design, but would have to be to achieve commercial status.

2.2.5 Phase Noise

RMS Cumulative Phase Noise ..... 0.2°

The synthetic range profile defined in Equation A.2 assumes precise frequency steps, Δf. Any frequency deviation from $f_i = f_0 + i\Delta f$ due to frequency instability in the synthesizer produces a reduction of the processing gain. In this section the effect of frequency instability on stepped frequency radar will be shown.

Effect of Frequency Instability on Stepped Frequency Radar

Step to step frequency deviation of the transmitted stepped frequency sequence results in a reduction of the peaks in the synthetic range profile and an increase in the noise level. G_i, defined in Equation 2.7, is the baseband

response from a target in the ith frequency step with a random phase error of $2\pi x_i \tau$ produced by the the random frequency error, x_i, and accumulated during the delay, τ, where x_i is defined as

$$x_i = \frac{\theta(t+\tau) - \theta(\tau)}{2\pi\tau} \tag{2.6}$$

and $\tau = 2R/c$.

$$G_i = e^{j\left(-2\pi f \frac{2R}{c} - 2\pi\tau x_i\right)} \tag{2.7}$$

[37] shows that for n frequency steps

(i) the expected value of peaks of the synthetic range profile is

$$E[H_l(x_i)] = nC_f \tag{2.8}$$

and

(ii) the variance at the null positions is

$$\sigma^2[H_l(x_i)] = nC_f^2\left[1 - C_f^2\right] \tag{2.9}$$

where

$$C_f = e^{-\frac{\sigma_c^2}{2}} \tag{2.10}$$

The expected ratio of peak signal to variance from 2.8 and 2.9 is

$$\frac{S}{\sigma_H^2} = \frac{n}{1 - C_f^2} \tag{2.11}$$

where the peak signal power is $S = (nC_f)^2$. The cumulative phase noise can be determined using one of the techniques presented in Appendix B. This can be incorporated in the loss factor in Equation 2.5 of the previous section.

To achieve a dynamic range in the synthetic range profile of 70dB, the cumulative phase noise, σ_c, of the synthesizer must be less than 3.74×10^{-3} radians (RMS) or 0.2 degrees for 140 frequency steps.

Effect of Frequency Instability and RF Components

Radio frequency components are characterised by scattering parameters (s-parameters). For well designed amplifiers, the parameter of most interest to the system designer is S_{21} which is a complex number that describes the forward transmission response with the output port terminated in a matched

Table 2.1: SCA-14S_{21} Data

Frequency [MHz]	**Magnitude** [dB]	**Phase** [°]
100	10.1	170
500	9.8	131
900	9.4	93
1000	9.3	84
1500	8.8	39

load as function of frequency. The magnitude $|S_{21}|^2$ is the transducer power gain into the a matched load. The phase $\angle S_{21}$ is the amount a signal of a particular frequency will be phase shifted. The S_{21} data the SCA-14 amplifier from Stanford Microdevices is shown in Table 2.1 below. It can be seen that the phase shift decreases approximately linearly with increasing frequency. This phase shift can be characterised by the phase delay of the amplifier which can be calculated from the s-parameter data. Using a least squares approximation to fit this data to a straight line, the $\angle S_{21}$ values for 200MHz and 1600MHz are 159.6° and 28.5° respectively. Thus the phase delay is $(159.6° - 28.5°)/1400\text{MHz} = 2.3\text{rad}/1400\text{MHz} = 1.6\text{ns}$.

Frequency deviations in the synthesizers calculated from the Allan variance, will be subject to differing phase shifts by the amplifiers. A frequency deviation of 10kHz on a signal passed through the amplifier will cause a phase deviation of 16×10^{-6} radians or 0.92×10^{-3} degrees. This is very much smaller than the cumulative phase error from the instability. Thus for small frequency deviations, the phase shift of the amplifiers will not impact on the performance of the radar.

2.2.6 Synthesizer Step Time

Step Time ..... $< 62\mu s$

The synthesizer step time is the time taken for the synthesizer to change from one frequency to another. This time will vary based on the size of the frequency step, but for the purposes of this specification parameter definition, will be the maximum step time.

The synthesizer step time added to the data capture time and data transmission time, must sum to less than that to achieve the number of scans per minute of 10.

The data capture time is calculated with a 2.667MHz sampling frequency (375ns sample time). Each frequency requires four samples to calculate the I and Q values. Each 4 sample set is recorded 256 times for averaging. Therefore the total number of samples is 1024 for each frequency with averaging. For 140 frequency steps, the total data capture time is 53.76ms.

The data capture time can be approximately calculated as follows. Assuming 140 transmitted frequencies, two values per frequency (I and Q) and two bytes for each value, the amount of data to be transmitted per frequency scan will be 560 bytes. Using a 10 bit per byte communications protocol (1 start bit, 8 data bits and 1 stop bit) and a transfer rate of 115200 bit per second, the data transfer time will be 48.61ms.

Thus the total capture and data transmission time is 102.4ms, which means that maximum possible number of number of scans per minute will be 9. The specification of 10 scans per minute can therefore not be met. However, to keep the number of scans per minute to 9, the time taken to step through all frequencies must be less than 8.70ms, which keeps the total pulse repetition time less than 111.1ms (9 scans per second). Thus the synthesizer step time must be less than 62μs.

2.2.7 Power Levels

RF Output ..... -15dBm to 15dBm

The radar output power level was determined by the maximum power that could be obtained from a surface mounted power amplifier. The output variation parameter was determined from the variation that could be obtained from commercial RF variable attenuators.

Maximum RF Input ..... -25dBm

The maximum RF input was determined from typical maximum input power levels for commercial low noise amplifiers. These generally had an output power 1dB compression point of 0dBm and a gain of 20dB. It was recommended that the amplifier be used at greater than 5dB below its rated 1dB compression point. This specification parameter is based on the assumption that the input to the transceiver is a single gain stage. There will be other gain stages in the receiver after the initial low noise amplifier, but the 1dB compression point of these will not affect the maximum input RF signal. It is therefore valid to base this parameter on the single gain stage at the input to the receiver.

presents the laboratory measurements made to determine the performance of the transceiver. For each measurement, the measurement technique and limitations of the measurement equipment is described. The chapter concludes with a comparison of the system specifications and the measured results. Chapter 6 presents a discussion on the performance of the radar and the success of the design predictions. Recommendations on the use of the transceiver and for further improvements are made.

Appendix A briefly reviews the principles of stepped frequency radar and ground penetrating radar. Appendix B gives a brief overview of frequency instability definitions which have been used to describe the performance of the synthesizers. Appendix C derives the formulas for the description of the phase locked loop portion of the synthesizers from which the synthesizer performance was estimated. Appendix D describes the acceptance test procedure for the transceiver. For each test, the aim and method are presented. Appendix E shows results of two measurements taken with the radar.

1.2 Background

The history and growth of ground penetrating radar has been well documented in literature [7, 22]. Up until 1972, most of the work in this field was undertaken by research institutions and government agencies. Over the past 30 years, the applications for subsurface sensing have grown and today there are several companies producing commercial ground penetrating radars. A list of these can be found in Section 1.3 of this chapter. There are also several institutions with ongoing research into ground penetrating radar. Several of these are also listed in Section 1.3.

Ground penetrating radars are used in the detection of subsurface objects or dielectric interfaces. There are many applications of GPR [7, 23]. Examples include the location of underground pipes, voids, individual objects such as barrels and unexploded ordinances, investigation of geological structures, and integrity of man-made structures such as roads and pavements.

Most of the systems produced commercially and in the research institutions have been impulse radars. Impulse radars operate by transmitting a very narrow pulse of electromagnetic energy with a peak power of up to tens of kilowatts. This energy is reflected by dielectric discontinuities and received by the radar to produce a profile of the subsurface objects. These radar systems require large instantaneous bandwidth and power to obtain high resolutions, and fast analogue to digital converters to sample the short pulses. They also suffer from antenna ringing and are susceptible to radio frequency interference. A description of the impulse method can be found

in [12, 21].

Stepped frequency systems have been shown that not to be susceptible to these problems [14, 21]. They also have many practical advantages including high mean transmitter power, high receiver sensitivity and the potential for intrinsic safety. Several stepped frequency systems have been produced both commercially and by research institutions. However, stepped frequency, ground penetrating radar development has been limited by the relative expense and bulk in comparison with impulse systems. Noon [21] gives a comprehensive summary of these systems and the state of the research up to 1996.

In 1995, the University of Cape Town embarked on a project to produce a low cost, portable stepped frequency, continuous wave, ground penetrating radar [15]. By the beginning of 1996, a portable 485 - 765 MHz homodyne architecture system had been constructed [16]. In 1997, in conjunction with Reutech Radar Systems, a 0.9 - 2.1 GHz system had been constructed for land mine detection [17]. This system had a superior architecture using a dual synthesizer heterodyne design.

The work presented in this thesis forms part of the latest GPR system to be produced by the University of Cape Town. This system, named Mercury B, is based on the same architecture as the 0.9 - 2.1 GHz Mercury system, but improves upon the Mercury system with a larger relative bandwidth of the radar, a calibration channel, better system configuration and faster data acquisition with sample averaging for noise cancellation. This dissertation describes the Mercury B transceiver module.

1.3 Further References

In addition to the references cited in the bibliography, the following sources were used to obtain background information for the work presented.

With the advent of the world wide web as an advertising medium, web pages of companies producing GPR systems have come to reflect the current state of commercial systems. The following is a list of companies producing commercial systems and their World Wide Web Universal Resource Locators (URL). A more general list of GPR URL links can be found at

`http://diwww.epfl.ch/w3lami/detec/gprbookmarks.html`

and

`http://www.cssip.uq.edu.au/~noon/gprlist.html`.

This value of received power is justified through a simulation of a typical target in a medium. This simulation is similar to the that used to produce Figure 2.1, as the same radar and target parameters were used. Figure 2.2 shows the expected receive power versus depth for four mediums with different attenuation constants. It can be seen that targets very close to the ground will saturate the input amplifier, but this is unavoidable, as commercially available surface mount, low noise amplifiers have 1dB compression point values of around 0dBm, as mentioned above. Thus targets close to the surface will saturate the receiver. However, depth information can still be extracted from a saturated received signal to a certain extent.

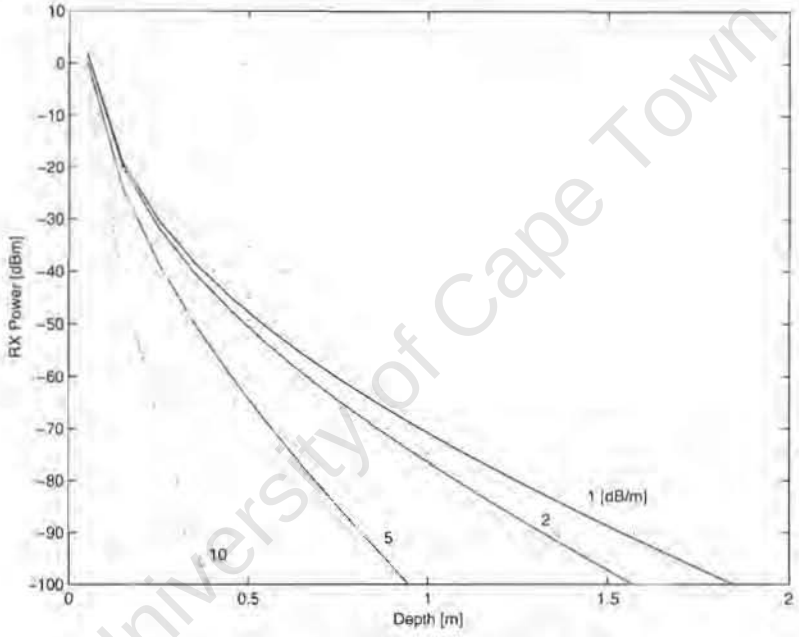

Figure 2.2: RX Power vs Depth

2.2.8 IF Characteristics

IF Center Frequency 2MHz

The IF center frequency was chosen as 2MHz to keep the IF bandpass filter physically small and also to keep the requirements on the sample and hold of the sampling ADC, cheap. The higher the IF frequency, the smaller the bandpass filter can be constructed. However, better and more expensive sample and hold ADCs are required, as this frequency is increased. It was found that 2MHz was a suitable compromise for commercially available

bandpass filters and samples and hold circuits of ADCs at present, and the budget available.

IF Bandwidth 100kHz

The bandwidth of the receiver is determined by the bandwidth of the bandpass filter in the IF chain as this filter will, in part determine the amount of noise power in the IF signal. The IF bandwidth was chosen to be large enough so that the settling time of the filter does not affect the pulse repetition time of the radar, but small enough so to keep the the noise power in the receiver to a minimum. A figure 100kHz was chosen as a reasonable compromise. The settling time of the filter is then be approximately 100μs.

IF Signal Power ..... $1V_{pp}$ (4dBm, 50Ω)

The required IF signal power requirement was specified by the the radar capture system input stage.

IF Harmonics ..... < -80dB

2.3 Mechanical

The transceiver motherboard will be 220mm in length and 100mm in width. It will connect to the backplane of the radar though a 96 pin DIN 41612 connector. It will house the daughter-boards to implement the frequency reference module, the transmit and local oscillator modules, and the RF and IF module. The daughter-boards will attach to the motherboard with double row IDC connectors and metal PCB spacers.

Chapter 3

Radar Design

The previous chapter developed the radar system specifications. This chapter will present radar design proposed to meet the specifications of the previous chapter. A combination of simulations and mathematical theory will be used to illustrate the advantages and disadvantages and performance of these designs.

The chapter begins with an investigation into possible radar architectures highlighting advantages and disadvantages of each. The synthesizer design will be presented and its performance shown. The design will be shown to have phase discontinuities over the synthesizer bandwidth. Also, the effect of the RF components on the phase of the received signal, due to wide bandwidth used in the radar, will be shown. Extensions to the architecture will then be presented to ensure transceiver coherency.

3.1 Transceiver Architectures

Several different architectures exist for the implementation of a stepped frequency radar. This section will review homodyne and heterodyne architectures, discussing the advantages and disadvantages of both.

3.1.1 Homodyne Systems

A homodyne radar is a system that synchronously detects a signal through the use of the original, transmitted signal. This is achieved by mixing the received signal with the a copy of the transmitted signal as shown in Figure 3.1. The output of the mixer contains information centered at both DC and

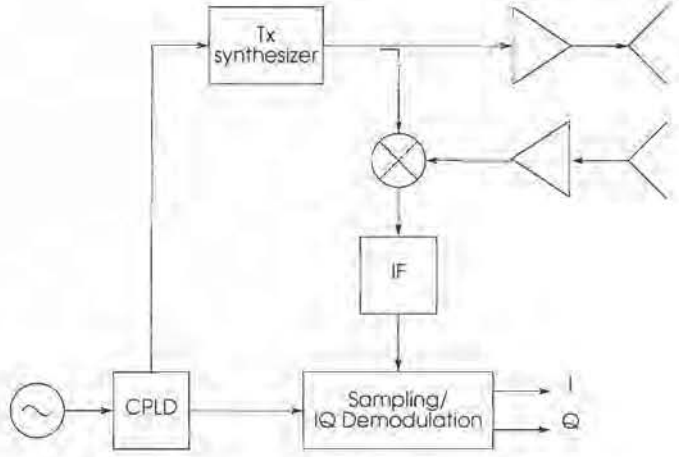

Figure 3.1: Homodyne Architecture

twice the transmitted signal. This signal is then low pass filtered to obtain the information from the DC component.

The above description of the homodyne system is purely theoretical. In practice, synthesizers do not produce a signal only at the carrier frequency, f_c, but due to non-linearities, harmonics at integer multiples of the carrier frequency. Re-evaluating the homodyne process including these harmonics, it can be seen that the harmonics, when multiplied by themselves, produce signals at DC. This is shown in Table 3.1 where each signal is represented by its frequency and f_c is the carrier frequency. Both the lower and upper sidebands are shown for the outputs of the mixer. Only the fundamental and the first two harmonics are shown here. From Equation A.2 it can be shown

Table 3.1: Mixer Output of Tx and Lo Signals

		Tx						
		f_c		$2f_c$		$3f_c$		$\cdots$
Lo	f_c	0	$2f_c$	f_c	$3f_c$	$2f_c$	$4f_c$	$\cdots$
	$2f_c$	$-f_c$	$3f_c$	0	$4f_c$	f_c	$5f_c$	$\cdots$
	$3f_c$	$-2f_c$	$4f_c$	$-f_c$	$5f_c$	0	$6f_c$	$\cdots$
	$\vdots$	$\vdots$		$\vdots$		$\vdots$		$\ddots$

that these signals produce targets in the synthetic range profile at integer multiples of the actual range to the target. To prevent this, the harmonics must be filtered before transmission, requiring filters operating at hundreds of megahertz and in many cases restricting the bandwidth of the radar to a single octave.

A further problem with homodyne systems arises from the extraction of the amplitude and phase from the received data. A quadrature demodulator is required to obtain the in- (I) and quadrature (Q) phase values. This requires a local oscillator, a quadrature detector module and analogue to digital converters for both I and Q channels. This system is prone to introducing gain and phase imbalances (or I and Q errors) through the quadrature demodulator and the analogue to digital converters which cause effects described in the previous chapter.

Finally, the DC signal in the homodyne receiver is subject to flicker noise and temperature variation. Although in general homodyne systems require less components and therefore have a lower production cost than heterodyne systems, they suffer from problems difficult to solve effectively.

3.1.2 Heterodyne Systems

A heterodyne radar is a system that synchronously detects a signal through the use of a signal that is offset in frequency from the transmitted signal by an intermediate frequency. This is shown in Figure 3.2. A homodyne system is thus really a heterodyne system with an intermediate frequency of 0Hz. Thus, it can be seen that a heterodyne system, by having a non 0Hz intermediate frequency, alleviates the problems of temperature drift and flicker noise associated with extracting measurements from DC signals. A

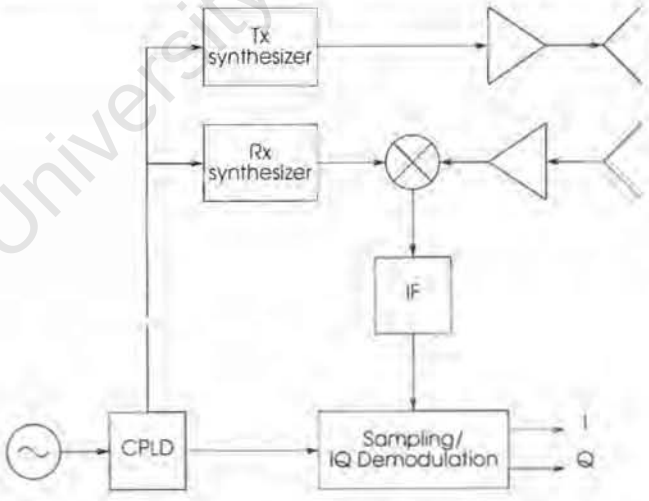

Figure 3.2: Heterodyne Architecture

further advantage provided by the heterodyne system is that the harmonics generated by the synthesizers are not required to be filtered before transmission as they mix down to outside the intermediate frequency bandwidth, as shown in Table 3.2 where f_{if} is the intermediate frequency. The format

of this table is similar to Table 3.1 except that only the lower sideband is shown for each of the outputs. However, it can be seen that instead of the harmonics mixing down to the intermediate frequency, they mix to integer multiples of the intermediate frequency. These can be effectively filtered by appropriate IF stage filtering. Extracting the I and Q values from the

Table 3.2: Mixer Output (LSB)

		Tx			
		f_c	$2f_c$	$3f_c$	$\cdots$
Lo	$f_c + f_{if}$	f_{if}	$f_c - f_{if}$	$2f_c - f_{if}$	$\cdots$
	$2(f_c + f_{if})$	$-f_c - 2f_{if}$	$2f_{if}$	$f_c - 2f_{if}$	$\cdots$
	$3(f_c + f_{if})$	$-2f_c - 3f_{if}$	$-f_c - 3f_{if}$	$3f_{if}$	$\cdots$
	$\vdots$	$\vdots$	$\vdots$	$\vdots$	$\ddots$

intermediate frequency can be achieved digitally by direct IF sampling and digital quadrature demodulation [36, 28, 35, 18, 11, 39, 38, 6]. However, the techniques presented in these papers refer to wideband IF signals. The intermediate frequency signal in this radar is a single frequency, these wideband techniques are not necessary in this system. This method also solves the IQ unbalance problem associated with quadrature demodulators.

A disadvantage of the heterodyne architecture is that it requires two frequency synthesizers as shown in Figure 3.2. These synthesizers must be phase locked to each other so as to maintain transceiver coherency. The design of the frequency synthesizers will now be presented.

3.2 Frequency Synthesizers

Section 2.2.5 highlighted several effects of frequency instability on the radar performance. The most severe effect was the reduction in the dynamic range of the synthetic range profile, which has the effect of masking smaller targets. To prevent these factors, the stability of the frequency source is crucial. A review of frequency synthesis techniques can be found in [19, 33, 30, 1].

Recently, digitally controlled, phase locked loop frequency synthesizer integrated circuits have become available. These make high performance stepped frequency synthesizer implementation viable. Direct digital synthesizers provide an easier method of frequency synthesis. They have output phase noise spectrum as good as that of the master oscillator and require little peripheral circuitry. However, these devices are currently limited to the 300MHz region and thus are only suitable for low frequency operation

(< 300MHz) unless direct frequency multiplication is used. This is undesirable as direct frequency multiplication increases the phase noise of the signal. Indirect frequency multiplication, as in phase locked loops, also causes an increase in phase noise, both the region over which this increase occurs and the amount can be controlled through design.

The frequency synthesizers were therefore chosen to be implemented as digitally controlled phase locked loops. A block diagram of the synthesizer design is shown in Figure 3.3. Phase locked loops are characterized by several factors which specify their performance. These are: frequency stability, spectral purity, step time and frequency step size. The rest of this section will describe the each of the synthesizer performance factors showing where they meet the specifications set out in the previous chapter.

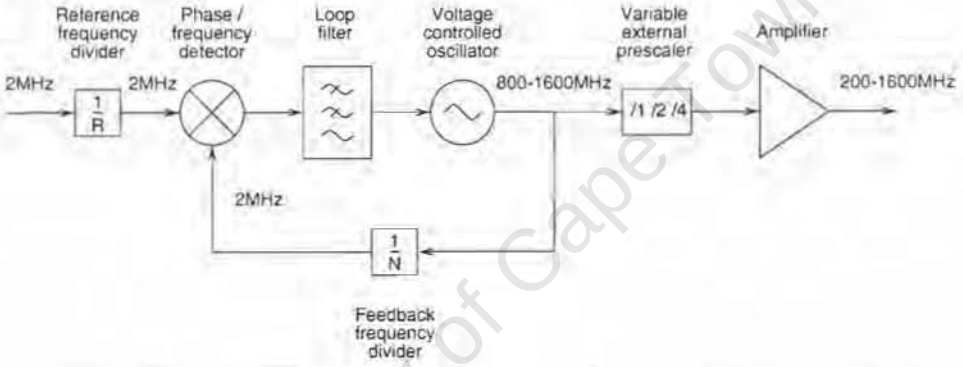

Figure 3.3: Overview Block Diagram of Frequency Synthesizer

3.2.1 Phase Locked Loop Parameters

Appendix C describes the model used to simulate the phase locked loop. Table 3.3 shows the parameters of the phase locked loop used to produce the simulation results. These parameters are those of the radar synthesizers, with the exception of the loop bandwidth, which shall be optimized to reduce the noise in the IF bandwidth. Also notice that the loop output frequency is 800-1600MHz which is the VCO frequency range. This will be translated outside the loop to 200-1600MHz.

3.2.2 Frequency Instability

Figures 3.4 and 3.5 show the predicted phase noise from the frequency synthesizer of the radar. The phase noise is measured in dB relative to rad^2/Hz and is known as the single sideband phase noise. The upper dashed line in

Table 3.3: Phase Locked Loop Parameters

Parameter	Value
Minimum loop frequency	800 MHz
Maximum loop frequency	1600 MHz
VCO tuning voltage constant	80 Hz/μV
Phase detector gain	0.302 V/rad
Phase detector frequency	2 MHz
Phase margin	44.5°
Open loop bandwidth	50 kHz
Closed loop bandwidth	79.7 kHz

Figure 3.4 is the phase noise contribution from the voltage controlled oscillator (VCO) and the lower dashed line, the phase noise contribution from the reference oscillator. The solid line shows the phase noise of the phase locked loop.

From the phase noise plot in Figure 3.4 the phase noise integrated over a particular bandwidth can be calculated using the techniques presented in Appendix B. For the data above, the the root mean squared phase jitter in radians over the band from 10Hz to 100kHz is 0.033 radians (1.9 degrees) . Assuming the same phase noise on the IF stage, this cumulative phase noise is greater than the required cumulative phase noise to achieve a 70dB dynamic range in the synthetic range profile, and corresponds to a dynamic range of 51.1dB. This does not meet the system specification, but will be used with a view for improvement in the future.

3.2.3 Spectral Purity

The frequency synthesizers must produce spectrally pure signals to avoid the generation of in-band intermodulation products at the output of the mixer, degrading the target detection performance of the radar.

An important consideration in designing phase locked loops is the suppression of the reference sidebands that are generated by the modulation of the VCO by the output of the phase/frequency detector. These can mix into the IF bandwidth and cause an amplitude and phase error to the target. They are usually close to the carrier and are thus hard to filter directly at the output of the synthesizer. However, by reducing the loop bandwidth these can be suppressed. This, however increases the settling time of the loop. Thus the loop bandwidth must be chosen to provide the required reference suppression, but also an acceptable loop settling time. The reference

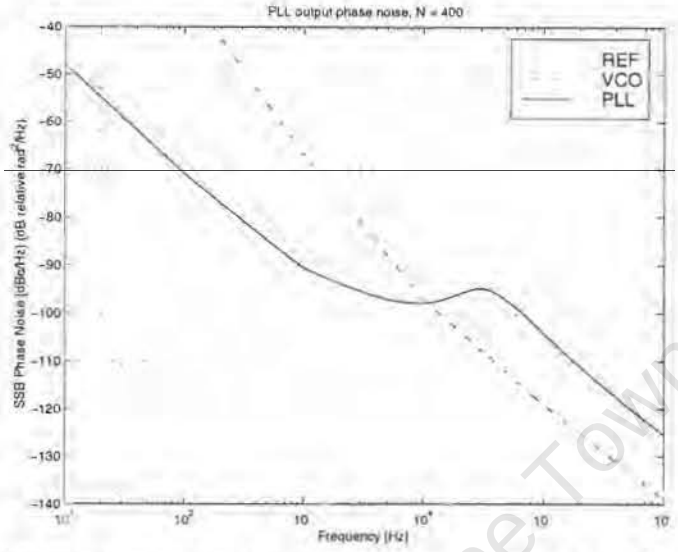

Figure 3.4: PLL Frequency Synthesizer SSB Phase Noise

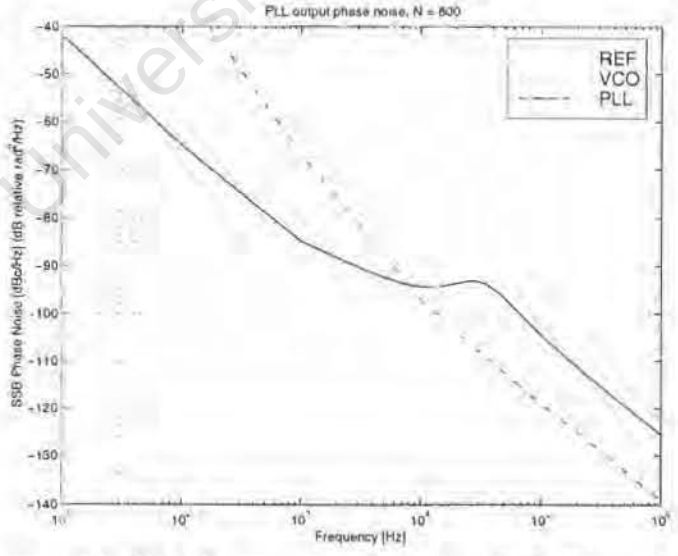

Figure 3.5: PLL Frequency Synthesizer SSB Phase Noise

sideband suppression calculated by the simulation is 57dB. This meets the system specification that all harmonics be less than 3dB below the carrier as the reference harmonics fall outside the IF bandwidth.

The voltage controlled oscillator (VCO) in the PLL synthesizers generate harmonics of the fundamental frequency due to inherent non-linearities. In most cases it is unnecessary to filter these unwanted harmonics before transmission as they usually mix out of the IF band.

Harmonics are not only caused by the PLL and VCO, but are generated by any non-linear device in the system. Usually third-order intermodulation products from mixers cause unwanted harmonics. However, these can also arise from devices such as amplifiers operating outside their linear region.

One further source of impurities in the transmitted signal arises from digital switching of the microcontroller. With careful board layout, isolation filters and decoupling capacitors, this can be minimized.

3.2.4 Step Time

The synthesizers use a single loop digital Phase-Locked Loop (PLL) technique for frequency synthesis. The PLL loop bandwidth therefore specifies the lock time and thus step time of the synthesizers. Increasing the loop bandwidth decreases the step time, which is a desirable feature. However, this also decreases the attenuation of the uncorrelated noise of the VCO and loop filter within the loop bandwidth. This is an undesirable feature, not only because of an increase in the noise level, but also because the noise in the IF signal of the transceiver will not correlate with the noise of the master oscillator. This will affect the sampling process which is controlled by the master oscillator as the mean squared values of uncorrelated noise sources add increasing the total noise. If on the other hand, the noise sources were correlated, the sampling timing would have the same noise characteristics as the received signal, thus reducing the effect of the frequency jitter due to the noise.

The lock time from the simulation varies across the bandwidth from 75μs to 83μs. However, the maximum step time occurs when stepping the VCO frequency from 800MHz to 1580MHz which occurs when stepping the radar frequency from 800MHz to 790MHz, and is about 120μs. This is the best that can be achieved while suppressing the reference harmonics by 57dB. This, however, does not meet the system specification of less than 62μs.

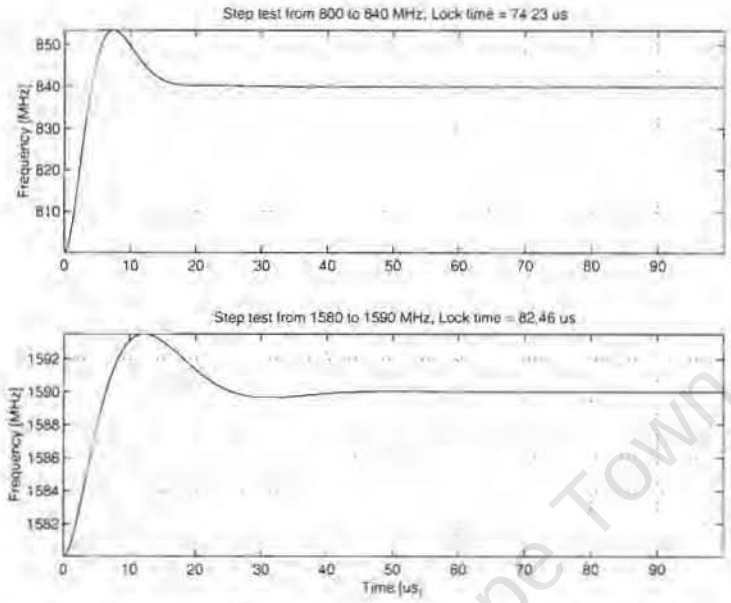

Figure 3.6: Synthesizer Lock Time Simulation 1

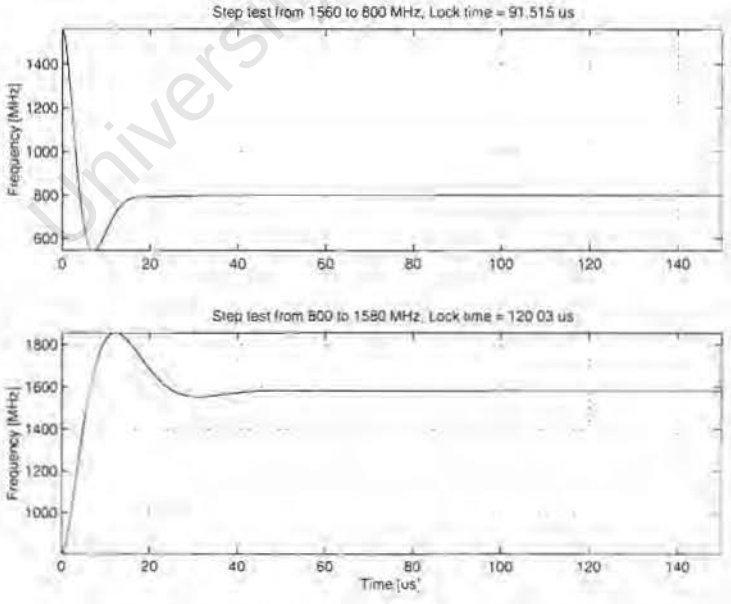

Figure 3.7: Synthesizer Lock Time Simulation 2

3.2.5 Frequency Step Size

The smallest step size of the synthesizer is specified by reference frequency applied to the phase detector of the PLL. It is desirable to have the PLL reference frequency as large as can be accommodated by the synthesizer IC, as loop filter will be more effective in suppressing the reference frequency feed through to the output of the synthesizers. However, the smallest step size across the band will determine the intermediate frequency of the radar. As direct IF down conversion is employed, it is recommended that the intermediate frequency be kept as low as possible, as the higher the IF frequency, the worse the signal to noise performance of the analogue to digital converter. A large reference frequency also implies a large phase detector frequency which is required to be filtered by the loop filter to produce the control voltage for the VCO. A higher phase detector frequency adds to the frequency requirements of the operational amplifier used to implement the loop filter.

3.2.6 Loop Filter Design

The loop filter is implemented as a differential active filter. The design of the loop filter is explained in [24, 25, 26, 27]. Przedpelski [25] presents a technique of optimizing a type-2, third order phase locked loop based on a chosen phase margin. Appendix C presents the structure of the loop filter, and the analysis to show the equivalence of the differential filter used in the synthesizer design and the design used in [24].

3.3 Transceiver Coherency

Stepped frequency radar relies on the measurement of the phase difference between the transmitted and received signals. To measure this phase difference, there must be a reference of the transmitted signal's phase. In general, radar coherency relies on the synthesizers and the sampling process being synchronized to the same master oscillator. This ensures that the phase measured in the intermediate frequency channel can be related back to the transmitted signal and therefore the phase difference measured.

The synthesizer design will not necessarily ensure that the synthesizers remain phase locked to each other due to the nature of the digital dividers. Two digital dividers exist in the synthesizers. The dividers are the phase locked loop reference divider of the frequency synthesizer integrated circuit and the output prescalers. The random phase change due to each will be shown separately and then modifications to the architecture will be pre-

sented to compensate for this phase corruption.

The section will conclude with a brief description of another source of phase corruption due to the RF amplifiers.

3.3.1 Reference Frequency Divider Phase Corruption (PLL IC)

The transmit and local oscillator synthesizers will be phase locked to the a reference frequency. This reference frequency (phase locked loop phase detector frequency) is generated by dividing down the master oscillator with a digital divider. A digital divider starts counting on either a rising or falling edge depending on the divider. Many clock edges of the master oscillator occur within a period of the reference frequency. If the dividers do not start dividing on the same edge of the master oscillator there will be a phase difference between the dividers' outputs, proportional to an integer number of masters oscillator periods.

The received signal is written mathematically in Equation 3.1 and the local oscillator frequency in Equation 3.2.

$$y_{rx} = cos\left[2\pi f_c\left(t - mT_{mo}\right) + \phi\left(d\right)\right] \tag{3.1}$$

$$y_{lo} = cos\left[2\pi\left(f_c + f_{if}\right)\left(t - nT_{mo}\right)\right] \tag{3.2}$$

m and n are the integer number of master oscillator periods that the received signal (transmit synthesizer) and the local oscillator are phase shifted. $\phi\left(d\right)$ is the phase due to the distance to the target. f_c is the carrier transmit frequency, f_{if} is the intermediate frequency and T_{mo} is the master oscillator period.

The output of mixing and filtering the IF output is given in Equation 3.3.

$$y_{if} = cos\left[-2\pi f_{if}t + 2\pi f_c\left(n - m\right)T_{mo} + 2\pi f_{if}nT_{mo} + \phi\left(d\right)\right] \tag{3.3}$$

Substituting $f_c = Nf_{if}$, $T_{mo} = 1/Rf_{if}$ where N is and R are integers (respectively the phase locked loop feedback and reference dividers) Equation 3.3 becomes

$$y_{if} = cos\left[-2\pi f_{if}t + 2\pi N f_{if}\left(n - m\right)\frac{1}{Rf_{if}} + 2\pi f_{if}n\frac{1}{Rf_{if}} + \phi\left(d\right)\right] \tag{3.4}$$

which can be simplified to

$$y_{if} = cos\left[-2\pi f_{if}t + 2\pi\frac{1}{R}\left[N\left(n - m\right) + n\right] + \phi\left(d\right)\right] \tag{3.5}$$

It can be seen that the term $2\pi\left[N\left(n-m\right)+n\right]/R$ in Equation 3.5 will not always be an integer multiple of 2π. Therefore there will be a random phase introduced into the IF data which will be based on the reference dividers of the phase locked loops.

This problem can be solved by referencing the phase locked loops to the same reference frequency by externally dividing the master oscillator to the required frequency with a single reference divider.

3.3.2 /2, /4 Prescaler Phase Corruption

A similar situation as described in the previous section arises with the prescalers used to extend the bandwidth of the radar. The IF phase error caused by the prescalers is mathematically shown below. Equations 3.6 and 3.7 are the received and local oscillator signals respectively.

$$y_{rx} = cos\left[2\pi\frac{f_{stx}}{p}\left(t - mT_{stx}\right) + \phi\left(d\right)\right] \tag{3.6}$$

$$y_{lo} = cos\left[2\pi\frac{f_{slo}}{p}\left(t - nT_{slo}\right)\right] \tag{3.7}$$

where $f_{slo}/p = f_{stx}/p + f_{if}$, m and n are integers and p is the prescaler value of either 2 or 4.

The IF band output of the mixer will then be

$$y_{if} = cos\left[-2\pi f_{if}t + 2\pi\frac{f_{stx}}{p}\left(nT_{slo} - mTstx\right) + 2\pi f_{if}nT_{slo} + \phi\left(d\right)\right] \tag{3.8}$$

There will therefore be a phase error introduced by the prescalers which will change every time the prescalers' divide ratios are changed, further corrupting the phase information.

3.3.3 Effect of RF Components

Stepped frequency radar transmits frequencies over a wide bandwidth. As the phase response of the amplifier does not increase linearly with frequency, frequencies at opposite ends of the spectrum will be phase shifted by different amounts. This has the effect of corrupting the distance information obtained by the radar.

To illustrate this, the phase shifts of a chain of amplifiers were incorporated into the basic stepped frequency simulation. The amplifiers used were the SCA-14 (TX power stage), SNA-386 (low noise amplifier) and the SNA-186

(additional receiver amplification). The result was that a target at 2 meters appeared at 1.35 meters, which is 0.65 meters closer to the radar. The range resolution of the radar (1390MHz bandwidth) is 0.108 meters. The targets are therefore range shifted by six range bins. Figure 3.8 shows the result of the simulation in which a target was placed at 2 meters.

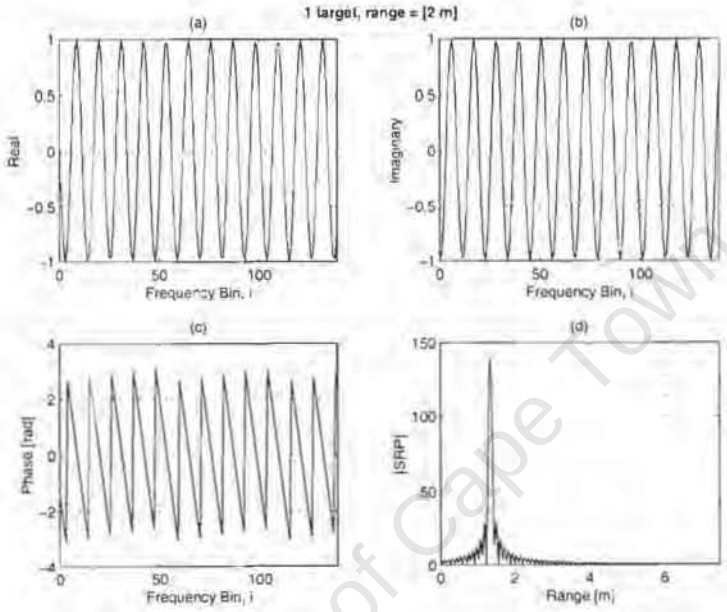

Figure 3.8: SF Radar Simulation (single target)

To compensate for this error, a calibration measurement though a cable of known length would have to be made to calculate the error in phase shift. This error could then be corrected in software processing.

3.3.4 Coherent Heterodyne Architectures

The problems introduced in the previous section can be solved by generating a reference intermediate frequency signal which contains only the phase error. This phase error can then be measured and for each received signal removed from the received signal using the reference measurement. Two options for generating this reference signal are shown in Figures 3.9 and 3.10. In Figure 3.9 a separate reference channel has been introduced to the system. The reference signal is generated by mixing signals coupled from the transmit and local oscillator synthesizers and sampling the band pass filtered result. This signal will then only contain the phase error present in the received data channel. However, as the reference and received channels use different components this system will suffer from component matching

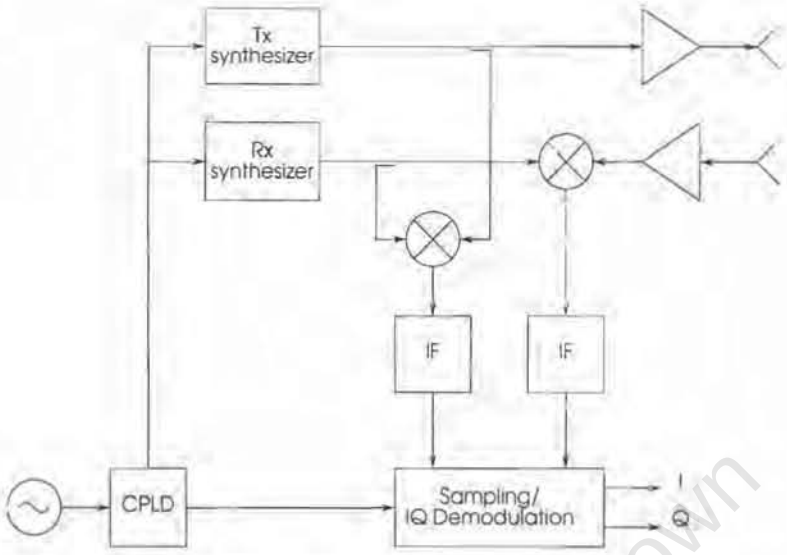

Figure 3.9: Dual Channel Heterodyne Architecture

errors which cause a phase difference between the channels, thus not canceling the phase error completely. Therefore it would be better to generate the reference signal through the same components used for the received signal. Figure 3.10 provides such a method.

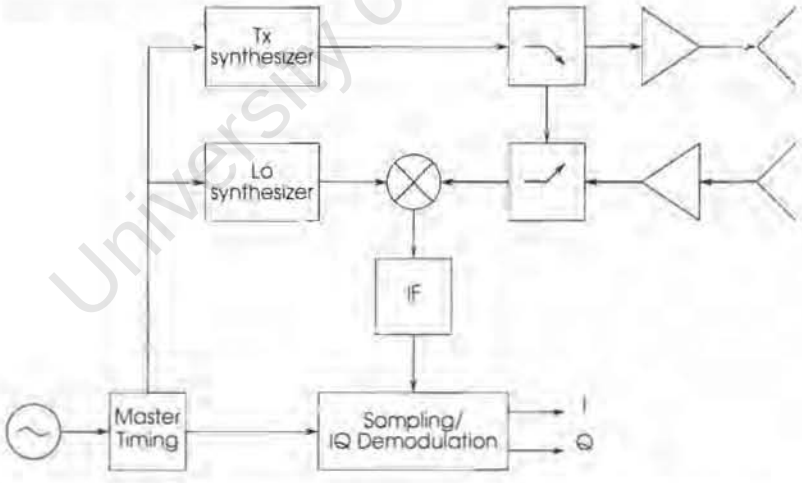

Figure 3.10: Interleaved Channel Heterodyne Architecture

In Figure 3.10, switches are used to either multiplex the received signal or the transmitted signal to the intermediate frequency hardware. The disadvantage of this is that the received and reference signals will be recorded in series which will take twice the amount of time. Also, the switches have a limited isolation. Therefore some of the alternate channel signal will couple through to the measured channel. However, this is controllable through the

choice of the switches. A typical value of 80dB of isolation can be achieved with two switches which meets the requirements for the harmonics in the IF bandwidth. Finally, as both signals are generated using the same hardware, the phase error between the received and reference channel will be minimized to the tolerances of a single set of components.

Chapter 4

Transceiver Implementation

This chapter describes the transceiver implementation detailing how the design of Chapter 3 was implemented. The chapter starts with an overview of the radar system. This is followed by a description of the mechanical construction of the transceiver. Each of the transceiver modules are then discussed in detail with specifications derived from the manufacturer data sheets. The chapter concludes with a brief analysis of the estimated power consumption of the system.

4.1 Radar Design Overview

This section presents a brief description of the radar to describe the environment in which the transceiver will operate. The radar can be divided into seven modules excluding peripherals such an odometer module. Each of these modules is listed and briefly described. The modules and their interconnections are shown in Figure 4.1.

- **Frequency Reference Module** (REF) or otherwise known as the master oscillator of the system. This module incorporates a crystal oscillator from which all radar signals and timing can be generated.
- **Radar Controller/Data Capture Module** (RCDC) controls the sequence of events in the radar in order to generate the radar signals and capture the data. The sequence of events is governed by a microcontroller implementing a communications protocol which allows the radar to communicate with an external personal computer. The data capture procedure is governed by a logic circuit which generates the timing from the master oscillator clock.

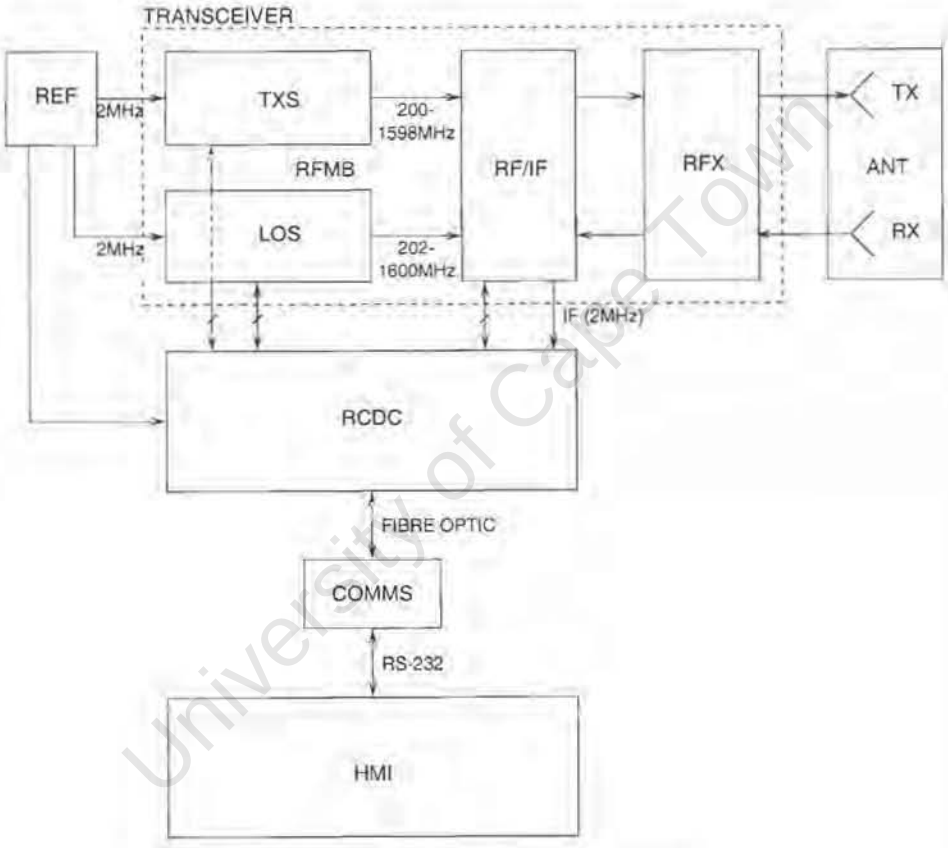

Figure 4.1: System Block Diagram

- **Communications Module** (COMMS) provides an optic fiber link from the radar to the personal computer. Optic fiber is used in order to isolate the radar electronics from the switching noise of the human machine interface computer. The communications module plugs into a standard 9 pin RS-232 port on the computer and links to the radar via fiber optic cables.

- **Human Machine Interface** (HMI) The human machine interface provides an interface to the radar. It enable the radar to be controlled and the radar data to be viewed in real time. Basic radar data processing is implemented for data viewing.

- **Transceiver Module** (TRANS) The radar transceiver consists of four modules which will briefly be described here. The rest of this chapter will then focus on the implementation of these modules. The dashed boxed region of Figure 4.1 shows the transceiver modules.

  - **RF Motherboard** (RFMB) attaches to the radar backplane and distributes power and data from the radar bus to the control lines of the each of the transceiver modules. The data bus is distributed though a complex logic programmable device.
  - **Transmit Synthesizer** (TXS) generates a low power version of the the radar signal for transmission. The synthesizer can be stepped in steps of 2MHz from 200MHz to 1600MHz.
  - **Local Oscillator Synthesizer** (LOS) is exactly the same as the transmit synthesizer in functionality, but generates the local oscillator signal to mix the received signal down to the intermediate frequency.
  - **RF/IF** (RFIF) implements the calibration channel and translates the received signal to the intermediate frequency.
  - **RF Extender Board** (RFX) currently provides the power amplification for the transmitted signal and the low noise amplification for the received signal. This board, however could be used to implement extensions to the radar RF electronics. Examples include a polarimetric switching network or configuration for a monostatic radar antenna arrangement.

- **Antennas** (ANT) The antenna design was outside the scope of this project.

- **Power Supply Unit** (PSU) The power supply unit converts a DC power supply of 9 to 18 volts to the required voltages for each of the modules of the radar. The voltages generated are +5V (RF), +9V, +24V, -5V and +5V (digital).

4.2 Mechanical Layout

The transceiver is divided into three daughter-board modules which plug into the transceiver motherboard. This transceiver motherboard is a 3U Eurocard with dimensions of 220mm by 100mm which plugs into the radar backplane. Figure 4.2 shows a photograph of the transceiver module in front of the radar.

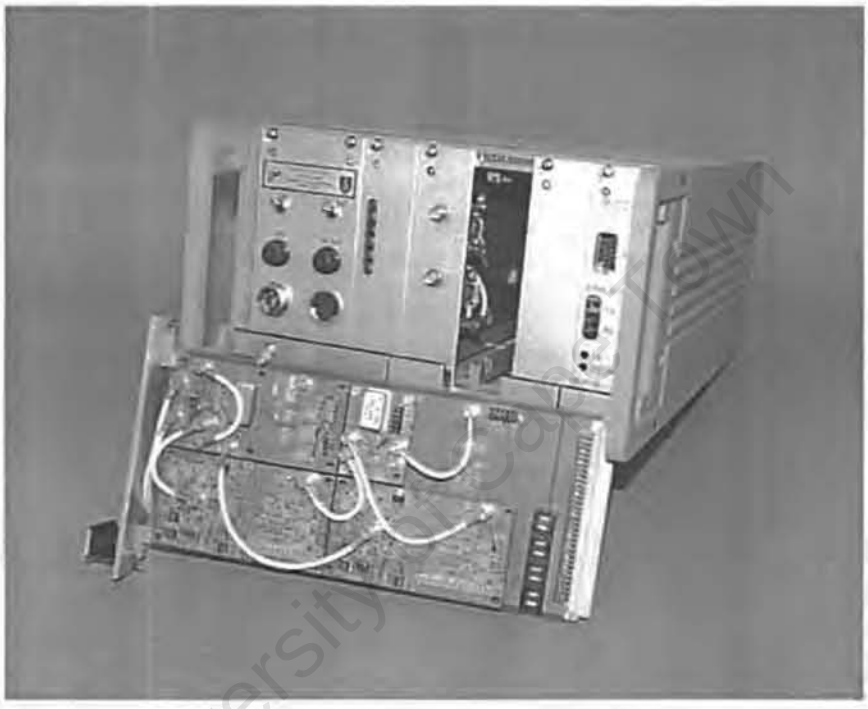

Figure 4.2: Transceiver Board and Radar

The transceiver daughter-boards plug into the motherboard via double row IDC headers and are secured by means of metal PCB spacers. These provide both mechanical stability to the daughter-board mounting, and also some radio frequency isolation between the boards. They also provide further ground paths from the motherboard to the daughter-boards which reduces current loops and therefore mutual coupling between systems.

The RF components are mounted on the bottom of the daughter-boards such that they face the motherboard. The motherboard is in turn flooded with ground plane. The electromagnetic energy generated by the daughter-boards will therefore couple onto this ground plane providing greater inter-board electromagnetic isolation.

The coaxial connectors feeding signals from each of the daughter-boards are mounted on the top which provides easy inter board connections. Suhner

Microax™ connectors were used for their size and ease of installation.

4.3 Transceiver Modules

The transceiver modules will be presented in this section. Each section will include a short description of the module supported by any important specifications and block diagrams. Due to commercial ventures concerning this radar system, the full schematics are unable to be published in the dissertation.

4.3.1 RF Motherboard (RFMB)

The function of the RF motherboard includes the distribution of power and control lines from the backplane to the transceiver daughter-boards. The translation from the backplane address and data buses to the control lines is achieved through a complex logic programmable device (CPLD). The CPLD functionality is defined with the hardware description language VHDL. The code for this device did not form part of the thesis requirements and was designed only in part by the author.

The RF motherboard also provides power supply filtering on the power supply lines from the backplane to reduce the amount of noise generated by the switching of the RCDC digital circuitry and PSU DC-DC converters.

4.3.2 Reference Oscillator Module (REF)

Although this module is strictly not part of the transceiver, it is physically located on the transceiver motherboard and some of its specifications, such as the phase noise, are used to calculate the performance of the other transceiver modules. Therefore it is included in this description of the transceiver modules.

The master oscillator is a 16MHz temperature compensated crystal oscillator with a HCMOS output. This is used to clock a complex logic programmable device which generates four clock frequencies through frequency division. The CPLD functionality is defined through VHDL. These outputs are in phase with the master oscillator and therefore each other. Two 2MHz outputs are generated for the synthesizer reference frequencies, one 4MHz signal to clock the RFMB CPLD and an 8MHz clock for the sampler (FPGA and ADC). The specifications for the crystal are given in Table 4.1.

Table 4.1: Master Oscillator Specifications

Nominal Frequency	16	MHz
Stability in the temperature range: 20°C to 70°C	$< \pm 2$	ppm
Current Consumption	< 20	mA
Output Voltage	HCMOS, low < 0.4, high > 4 (1kOhm, 15pF) 50%±10% 10ns rise/fall time	V
Phase Noise		
10Hz	-85	dBc
100Hz	-108	dBc
1kHz	-128	dBc
10kHz	-140	dBc
100kHz	-150	dBc
1MHz	-153	dBc

4.3.3 Synthesizer Module (TXS, LOS)

The synthesizers are single loop phase locked loops that use a frequency synthesizer integrated circuit to provide the reference and feedback dividers and the phase detector. The active loop filter provides the control signal for the voltage controlled oscillator. This is then buffered to reduce the loading of the VCO. The output of the phase locked loop is frequency divided to extend the band of the PLL and then passed through a variable attenuator to achieve a flat output spectrum. A block diagram of the synthesizer is shown in Figure 4.3. The maximum and minimum RF power levels are shown on each of the RF lines.

The phase locked loop integrated circuit implements a phase/frequency detector, a reference frequency divider, which was set to 1, and a feedback frequency divider. The phase/frequency detector outputs two signals, phase detector pulse up (PDU) and phase detector pulse down (PDD). PDU pulses high approximately 1.9V when the divided VCO lags the divided reference in frequency or phase. PDD pulses high when the divided VCO leads the divided reference in phase or frequency. Thus the phase error is encoded as a pulse width modulated waveform whose DC average is proportional to its duty cycle which equals the phase error. These signals are subtracted in a differential filter to produce the control voltage for the VCO.

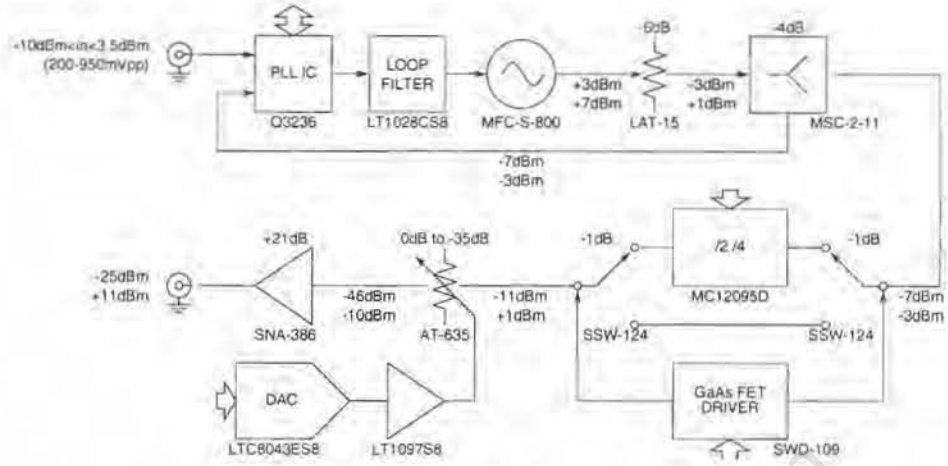

Figure 4.3: Synthesizer Block Diagram

The phase locked loop IC was chosen for its ability to divide the reference frequency by 1. The feedback frequency divide ratio was also important as it needed to be able to divide the feedback frequency to a relatively high phase detector frequency. The phase detector operates up to 100MHz, and the feedback divider to 2.0GHz. Three encoded bytes are sent to the phase locked loop to set the reference frequency and feedback frequency dividers. The reference frequency divider has a range of 1 to 63 and the feedback diver, 90 to 5135.

The loop filter circuit diagram is shown in Figure 4.4. Theorectical component values were calculated using the phase locked loop design program. These and the actual values used are shown in Table 4.2. The operational amplifier was chosen for its ultra low noise specifications and high gain bandwidth product. It has a maximum input noise voltage density of $1.1\text{nV}/\sqrt{\text{Hz}}$ and an input noise current density of $1.6\text{pA}/\sqrt{\text{Hz}}$, both at 1kHz offset frequecy. The gain bandwidth product is 20MHz for an input frequency of 200kHz. which is sufficient for the loop filter.

Table 4.2: Loop Filter Component Values

Component	Calculated Value	Actual Value	Unit
R1/2	263.697	240	Ω
R2	605.76	620	Ω
C1	10	10	nF
C2	12.686	10	nF

The voltage controlled oscillator used had a guaranteed operating frequency range of 800-1600MHz with a nominal tuning voltage of 0-20V. The speci-

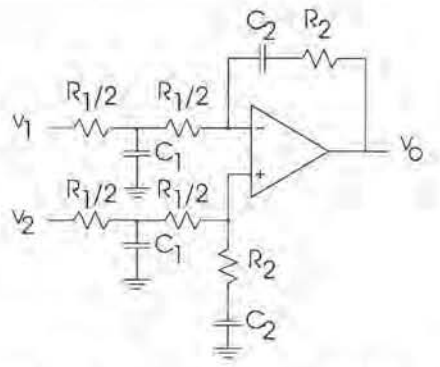

Figure 4.4: Loop Filter Circuit Diagram

fications are shown in Table 4.3.

Table 4.3: Voltage Controlled Oscillator Specifications

Frequency Range	800-1600	MHz
Tuning Voltage	0-20	V
Ouput Power	+5±2	dBm
Phase Noise	$f_c = 1.75351$	GHz
100 Hz	-35	dBc
1 kHz	-72	dBc
10 kHz	-100	dBc
100 kHz	-122	dBc
1 MHz	-142	dBc
10 MHz	-162	dBc
Typical Harmonic Suppression	10	dBc
Modulation Bandwidth	2.5	MHz

The output of the loop is divided by a variable divider (prescaler). This divides the frequency by either 2 or 4. The prescalers are used translate the output frequency of the phase locked loop (800-1600MHz) to the frequency range, 200-800MHz. However, by bypassing the prescalers (essentially divide by 1), the bandwidth of the system could be extended to 200-1600MHz. The prescalers also provide the capability of stepping the output frequency of the system in 1MHz steps over 400-800MHz and 500kHz steps over 200-400MHz.

The output power of the synthesizers are adjusted by a variable attenuator which is in turn controlled by a 12 bit digital to analogue converter (DAC). The DAC generates a negative voltage from 0 to -5V which controls the variable attenuator. To obtain a flat output power response over the band of the radar, the radar is required to be calibrated for each output frequency. This allows the same generic synthesizer module to be used for both the

TXS and LOS even though their output power level requirments are not the same. Therefore only a single version synthesizer module needs to be manufactured.

4.3.4 RF/IF Module (RFIF)

The RF/IF module implements the down-conversion of the received signal to the intermediate frequency, and the reference channel for phase correction. A block diagram of the RF/IF module is shown in Figure 4.5.

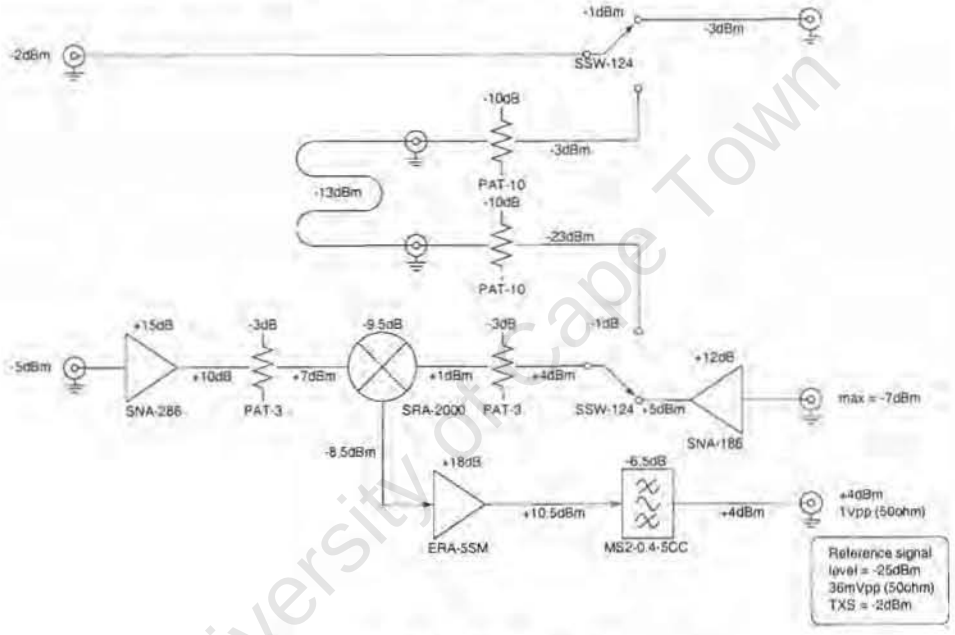

Figure 4.5: RF/IF Block Diagram

The maximum input signal level of the radar is determined by the maximum input power is to the mixer (+1dBm). Figure 4.5 shows the maximum levels for guaranteed operation through the receiever chain, and the IF level of the reference signal. The transceiver specifications were calculated from the component data sheets and these are listed in Table 4.4.

The reference channel is also shown in Figure 4.5. The phase of the transmit synthesizer is recorded by switching the transmitted signal to the receiver and mixing down to IF. This reference IF signal contains only the phase corruption of the /2/4 prescaler. Thus the phase of the received IF signal can be adjusted by the known phase corruption, thereby canceling the error.

The bandpass filter used in the implementation of the transceiver was custom made by Lark Engineering. The only specifications of the desired filter given

Table 4.4: Calculated Transceiver Specifications (25°C)

Receiver Noise Figure	4.1	dB
Maximum Receiver Input (with LNA from RFXRX module)	-28	dBm
Noise Floor	-119.8	dBm
Dynamic Range	91.8	dB

Lark Engineering were the center frequency of 2MHz, the -3dB bandwidth of 100kHz, the stopband level of -70dB at 1MHz from the center frequency and the input and output impedences of 50Ω.

4.3.5 RF Extender Module (RFX)

The RF extender (RFX) motherboard at present contains two daughter-boards which implement the transmit (RFXTX) and receive (RFXRX) gain stages. The motherboard connects to the backplane and supplies power to the daughter-boards. A block diagram of the RFX module is shown in Figure 4.6.

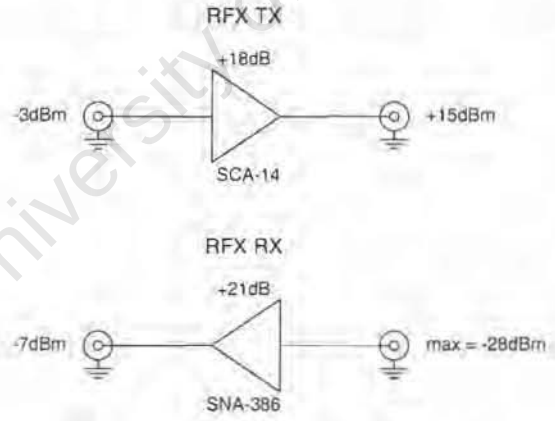

Figure 4.6: RFX Block Diagram

The RFX transmit daughter-board (RFX TX) amplifies the transmit synthesizer signal to the required output power level for transmission of the electromagnetic wave into the ground. This was achieved using a power amplifier.

The RFX receive daughter-board (RFX RX) amplifies the received signal with a low noise amplifer. The low noise amplifer was chosen with a low noise figure and high gain, which effectively sets the noise figure of the receiver.

4.4 Power Consumption

In order to design the power supply module, a current rating for each of the voltages generated by the PSU needed to be specified. The current consumption of each of the transceiver modules was calculated for each of the supply voltages from datasheets supplied by the component manufacturers. The maximum, and not typical, current ratings were used to calculate an upper bound on the current drawn. These values have been tabulated in Table 4.5. The modules are listed in the first column. The subsequent columns contain the currents associated with each of the supply voltages.

Table 4.5: Transceiver Current Consumption [mA]

Module	+5V	-5V	+9V	+24V	Total
RFMB	120	0	0	0	**120**
REF	90	0	0	0	**90**
TXS	206.1	14.5	73.1	12.5	**306.2**
LOS	206.1	14.5	73.1	12.5	**306.2**
RFIF	65	0	100	0	**165**
RFXTX	0	0	100	0	**100**
RFXRX	0	0	35	0	**35**
Total	**687.2**	**29**	**381.2**	**25**	**1122.4**

Chapter 5

Transceiver Laboratory Measurements

Laboratory measurements on the transceiver components were performed to check the operation of the tranceiver and to determine the tranceiver performance. The laboratory equipment used in the measurements of the transceiver are described in the first section of this chapter. The acceptance test procedure (ATP) and the transceiver operational tests performed according to the acceptance test procedure are then described and the results are shown. Finally the results of the performance measurements are presented. These performance measurements show whether the desgin meets the system specifications outlined in Chapter 2.

5.1 Measurement Equipment

5.1.1 HP8591A Spectrum Analyser

The spectrum analyser specifications are given presented in this section. The limitations on the measurements, due to these specifications will be described.

The spectrum analyser phase noise, at an offset frequency of 30kHz, is less than or equal to -95dBc/Hz. Thus, the phase noise of sources with phase noise levels lower than this value are not measurable with the spectrum analyser. Also, the accuacy of all phase noise measuements other than that at 30kHz will be uncertain, as it is the only specification given for the spectrum analyser. The frequency readout accuracy was given in the spectrum analyser data book.

Frequency Readout Accuracy = ±(frequency readout × frequency reference error + 3% of span + 20% of RBW + 1.5kHz)

where

Frequency Reference Error = aging rate × period of time since last adjustment + initial achievable accuracy + temperature stability

and

the initial achievable accuracy = $\pm 0.5 \times 10^{-6}$. the aging rate = $\pm 1 \times 10^{-7}$ and the temperature Stability = $\pm 5 \times 10^{-6}$.

Thus, assuming the spectrum analyser has never been calibated since purchase 10 years ago, the frequency readout accuracy on a signal at 1600MHz with a span of 10MHz and a resolution bandwidth of 1kHz, would be ±894.5kHz (1599.1055GHz to 1600.8945GHz).

5.1.2 Digital Oscilloscope

An HP54645D dual channel digital oscilloscope was used to record time domain waveforms in the radar. The HP54645D is digital mixed signal oscilloscope. It has two analogue 100MHz input signal channels with 200 MSamples/s sampling rate and 1 MB of memory per channel. The scope is used for timing measurements and has a time base accuracy of 0.01% of the time span, and a horizontal resolution of 40ps. The verticle resolution of the scope is 8 bits (256 values).

5.2 ATP Results

This section presents a summary of the the results of the acceptance test procedure described in Appendix D.

5.3 Received Channel Data

Chapter 3 described the effects of using a variable divide prescaler on the coherency of the system and thus the need for a reference phase measurement. Data captured from the reference channel is used to implement this phase correction. Figure 5.2 shows a radar measurement without phase correction. Clear phase discontinuities can be seen at 400MHz and 800MHz where the prescaler changes its divide ratio from 4 to 2 and from 2 to 1 respectively.

Table 5.1: ATP Results

Test	**Result**
Motherboard Power Test	*Passed*
Frequency Reference Power-On Test	I_{REF} = 27mA
Frequency Reference Operational Test	*Passed*
Synthesizer Power-On Test	I_{TXS} = 142mA
	I_{LOS} = 147mA
Voltage Controlled Oscillator Test	*Passed*
Phase Locked Loop IC Test	*Passed*
Synthesizer Lock Test	*Passed*
Variable Attenuator Test	*Passed*
Maximum/Minimum Output Power Test	Table 5.2
Constant Output Power Test	Figure 5.1
RFIF Power-On Test	I_{RFIF} = 160mA
Reference Channel Test	*Passed*
Receive Channel Test	*Unable to measure*
RFX TX Power-On Test	$I_{RFX\ TX}$ = 92mA
RFX TX Operation Test	*Passed*
RFX TX Maximum/Minimum Powe Level Test	Table 5.3
RFX RX Power-On Test	$I_{RFX\ TX}$ = 32mA
RFX RX Operation Test	*Passed*

Table 5.2: Maximum/Minimum Synthesizer Output Power

Frequency [MHz]	**Minimum [dBm]**	**Maximum [dBm]**
200	-22	+17
400	-19	+16
800	-21	+12
1590	-18	+6

Table 5.3: Maximum/Minimum RFX TX Output Power

Frequency [MHz]	**Minimum [dBm]**	**Maximum [dBm]**
200	-3	+18
400	-1.5	+16
800	-3	+12
1590	-2	+6

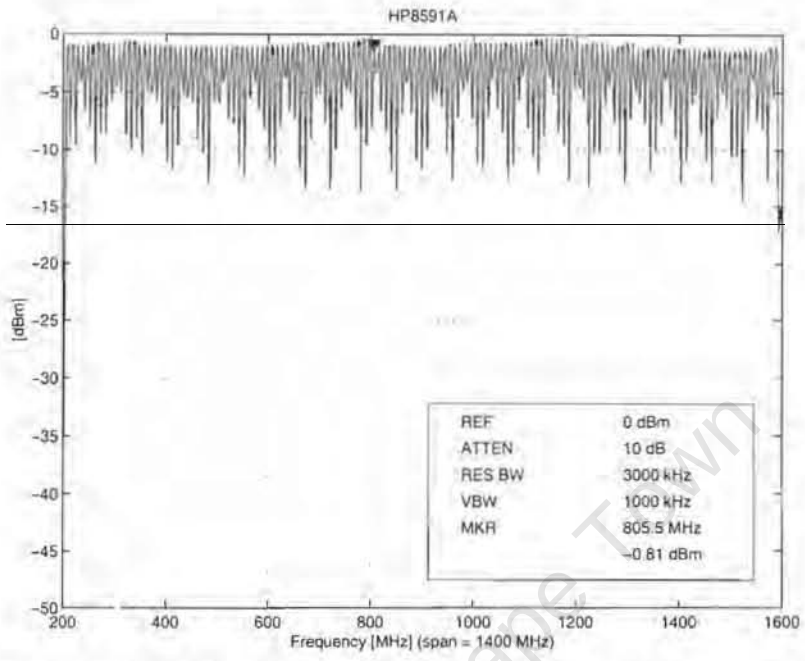

Figure 5.1: 200MHz to 1590MHz Synthesizer Frequency Spectrum Sweep

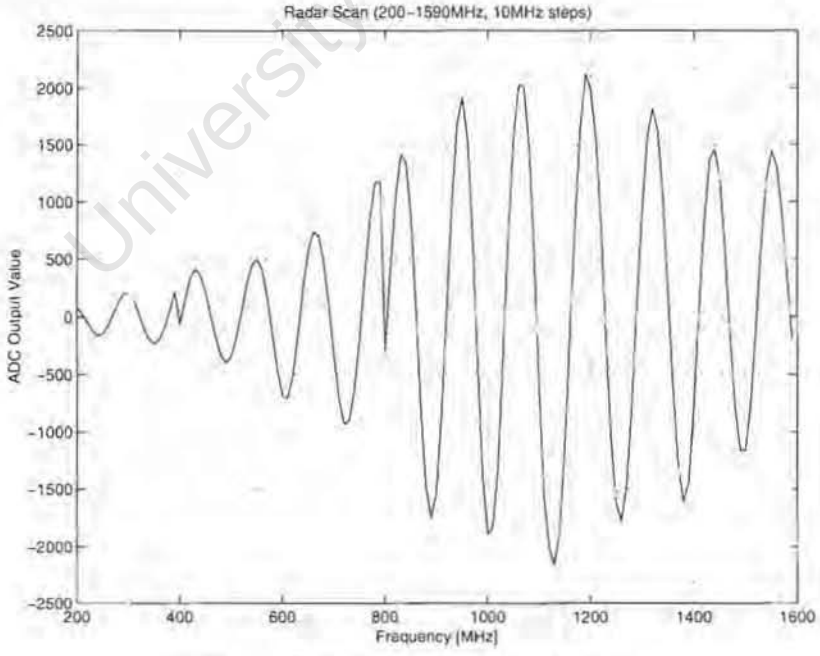

Figure 5.2: Receive Channel Data

It can also be seen that the amplitude of the received data increases for higher transmi. frequencies. In the phase correction procedure, the reference signal also corrects this amplitude difference as it has a similar amplitude variation across the band. This is shown in the first graph of Figure 5.3. However, Figure 5.3 also shows that for small attenuations, that is a high signal to noise ratio, the gain variations can be corrected to a reasonable degree. However, for large attenuations the gain variations in the received signal are unable to be corrected, especially at the received higher frequencies. The effect of this error in correction of the received data on the synthetic range profile is shown in Figure 5.4. It can be seen that for greater than 80dB attenuation, the amplitude and phase correction fails.

5.4 Dynamic Range Measurement

The dynamic range of the radar was calculated by measuring the minimum detectable signal and calculating the maximum input signal from component data sheets. The minimum detectable signal was measured by increasing the attenuation between the transmitter and the receiver, until the signal was buried in noise and could not be distinguished. The measurements show the dynamic range of the radar where each of the received samples has been recorded 256 times and averaged which is the standard operational mode for the radar. This averaging reduces the amplitude noise floor in the received data and thus improves the dynamic range.

Figure 5.5 shows that the minimum detectable signal occurs with a signal path attenuation of between 90dB to 100dB. The transmitted power was +15dBm, therefore the received signal was -75dBm to -85dBm. The maximum receiver input signal is calculated in Table 4.4 is -28dBm. Therefore the dynamic range of the system is greater than 47dB but less than 57dB.

5.5 Spectrum Measurements

The frequency spectrum of the each of the synthesizers were measured to show the frequency harmonics generated by the synthesizers and the reference harmonics of the phase locked loops.

5.5.1 Frequency Harmonics

Figures 5.6, 5.7 and 5.8 show the synthesizer spectrum at 200MHz, 400MHz and 800MHz respectively. The spectrum in Figure 5.6 (200MHz) has even

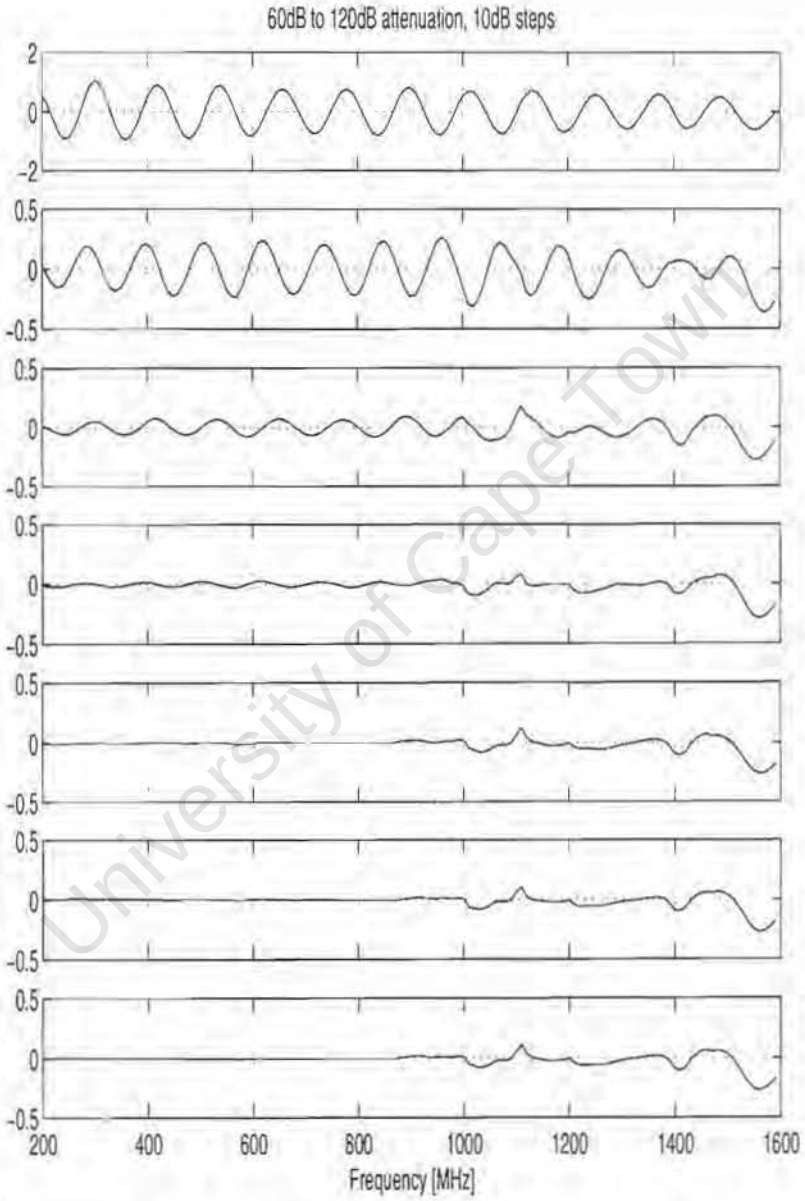

Figure 5.3: Spatial Frequency Domain Received Data

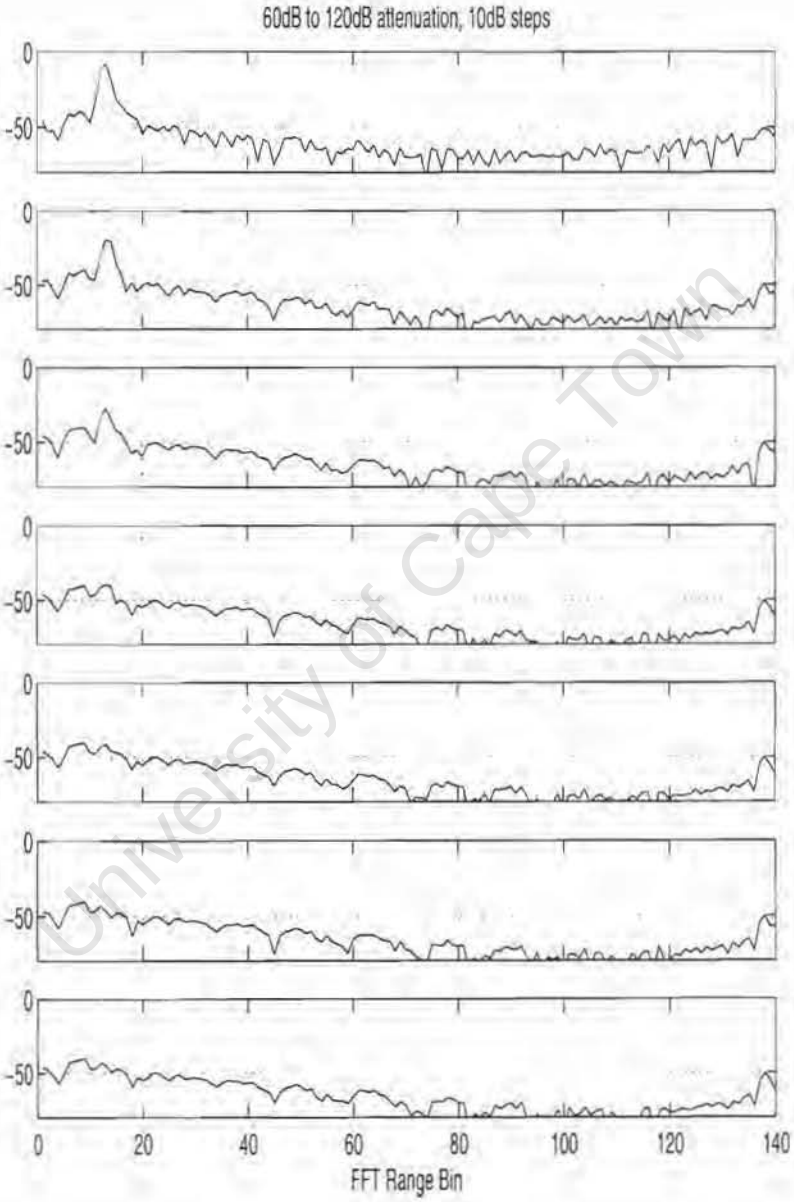

Figure 5.4: Spatial Time Domain Received Data

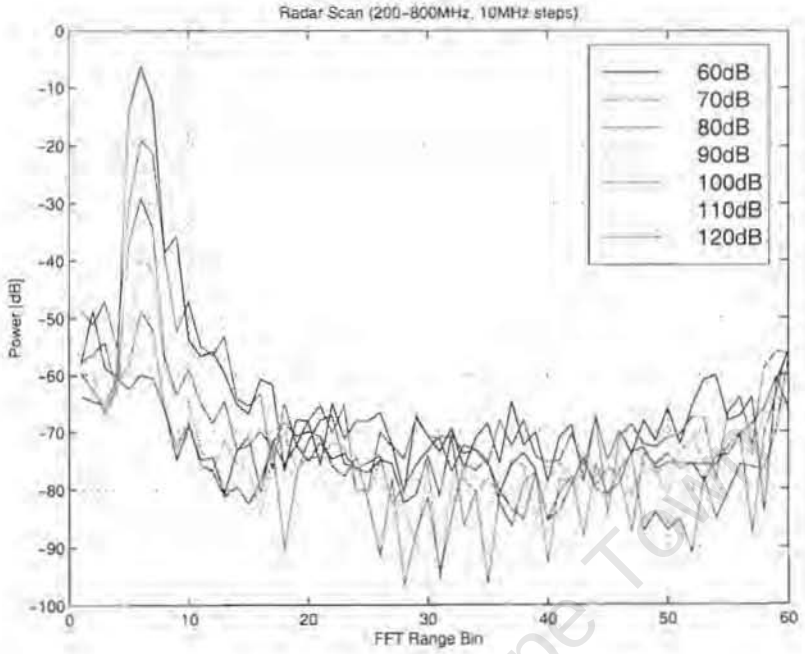

Figure 5.5: Minimum Detectable Signal

and odd harmonics which are generated by a combination of the harmonics from the VCO and the digital frequency prescaler that divides the frequency by 4. There are 7 harmonics in Figure 5.6. At a center frequency of 400MHz, the higher frequency harmonics have moved out of the upper end radar bandwidth leaving only 3 in the 200MHz to 1600MHz band. At above 800MHz, the hamonics have moved out of the bandwidth.

5.5.2 Reference Spurs

Figures 5.9, 5.10 and 5.11 show the reference frequency spurs from the phase locked loop at carrier frequencies of 200MHz, 800MHz and 1590MHz. The maximum predicted level of the reference spurs, given in Chapter 3, is 57dB below the carrier. In Figure 5.11 the reference spurs are at 55dB below the carrier which agrees with the prediction.

5.6 Phase Noise Measurements

This section presents the measurement of the phase noise of the synthesizers. The phase noise measurement technique and associated limitations are described, and then the results are presented.

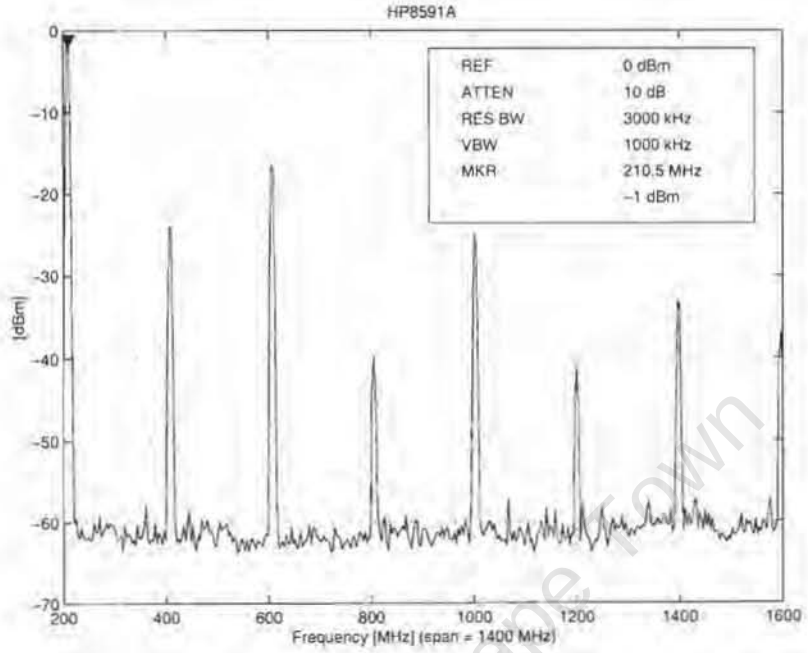

Figure 5.6: Synthesizer Frequency Spectrum, f_c=200MHz

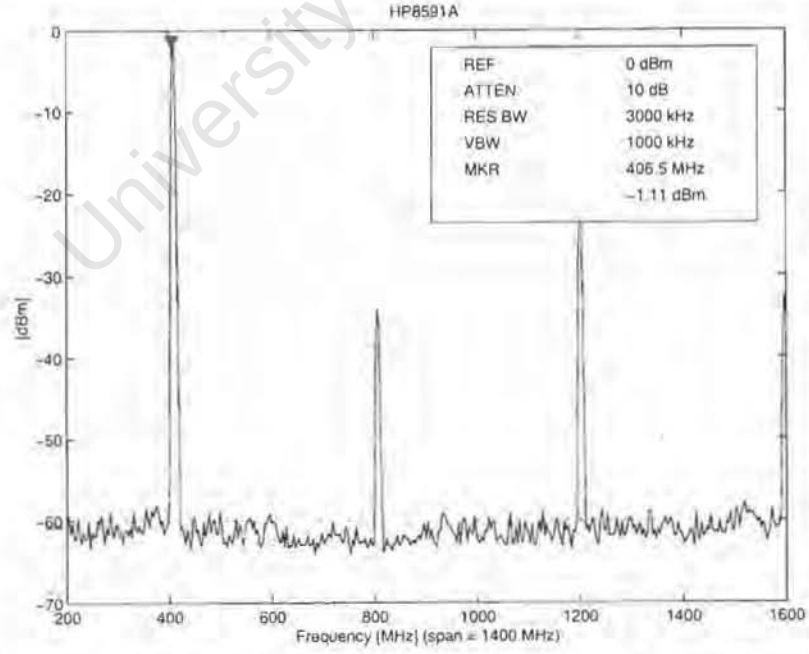

Figure 5.7: Synthesizer Frequency Spectrum, f_c=400MHz

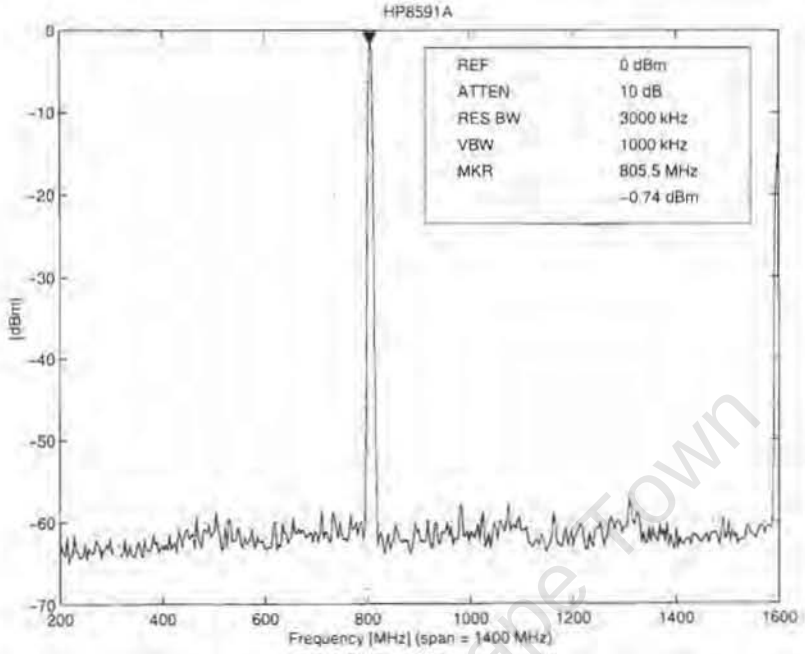

Figure 5.8: Synthesizer Frequency Spectrum, f_c=800MHz

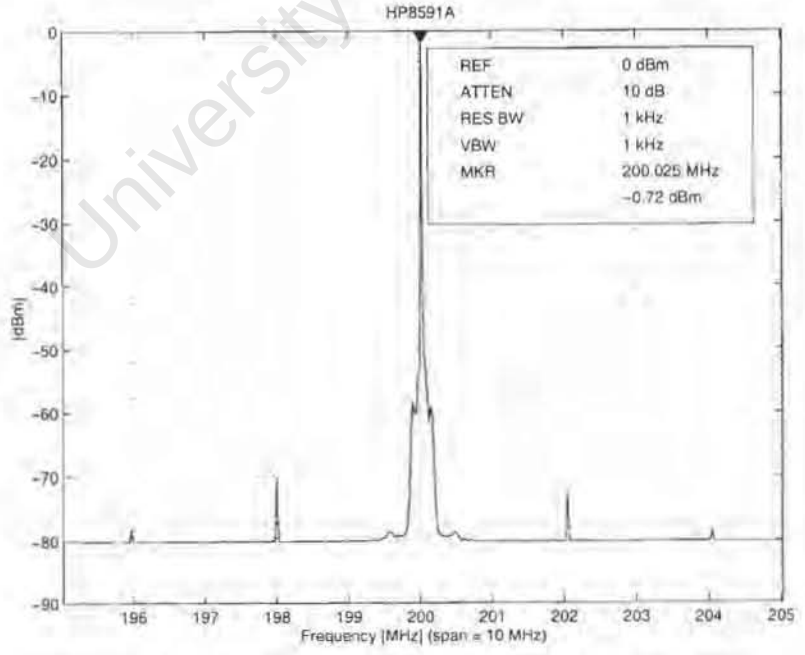

Figure 5.9: Synthesizer Reference Spurs, f_c=200MHz

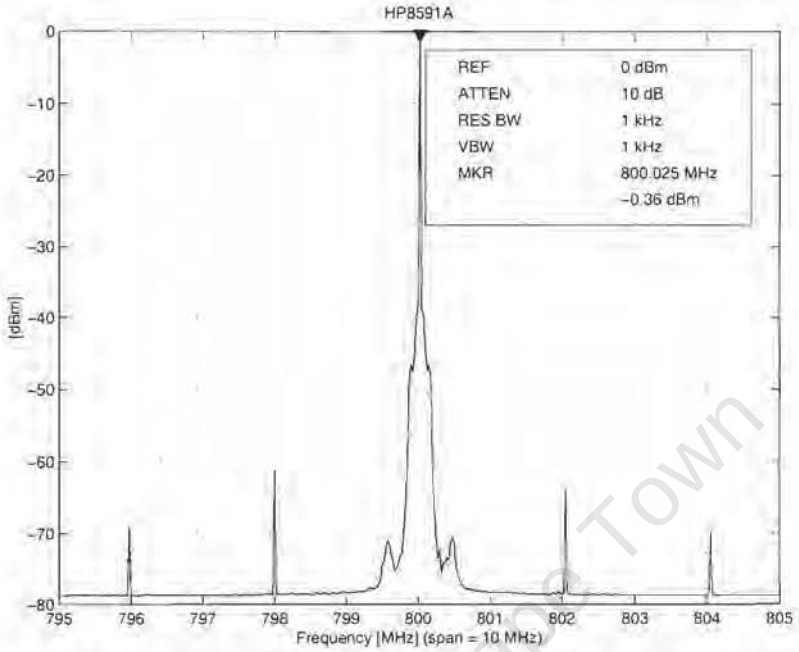

Figure 5.10: Synthesizer Reference Spurs, f_c=800MHz

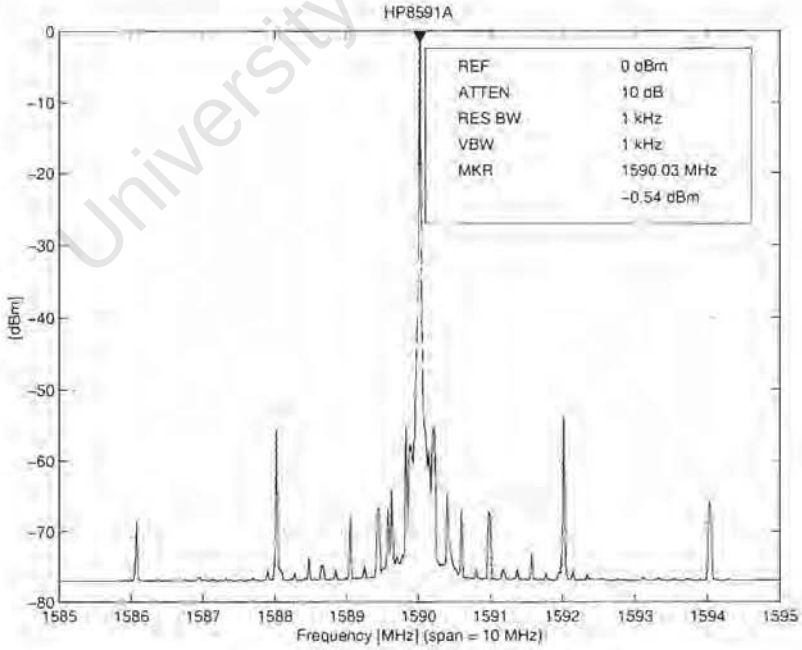

Figure 5.11: Synthesizer Reference Spurs, f_c=1590MHz

5.6.1 Phase Noise Measurement Technique

Due to limitations of the equipment available, approximate one sided power spectral density phase noise measurements were made using a technique with a spectrum analyser. This technique is described in [4] and is briefly explained here.

The spectrum analyser is tracks center frequency of the carrier signal and the span is adjusted so that the appropriate offset frequency can be viewed. To achieve the optimum results, the resolution bandwidth is set to the minimum in an attempt to achieve as close as possible to the 1Hz measurement bandwidth in the definition of the phase noise measurement.

The level shown by the spectrum analyser is actually the result of the integrated energy in the bandwidth specified by the resolution bandwidth. If the resolution bandwidth is sufficiently small, then it can be assumed that the energy is equal across the resolution bandwidth. Thus, to obtain the amount of noise energy in a 1Hz measurement cell, the measured value is divided by the value of the resolution bandwidth. Taking the logarithm of this, we obtain Equation 5.1.

The phase noise measurement is then the level of the noise at the offset frequency in decibels below the carrier minus ten times the logarithm to the base ten of the resolution bandwidth or

$$\mathcal{L}(f_m) \approx F(f_m) - 10\log_{10}(\text{RES BW}) \tag{5.1}$$

where $\mathcal{L}(f_m)$ is the single sideband phase noise at the offset frequency, f_m, $F(f_m)$ is the measured spectrum value at the offset frequency in decibels below the carrier and RES BW is the resolution bandwidth in hertz.

This measurement is only accurate if the phase noise of the spectrum analyser signal source is less than that of the synthesizer. If this is not the case, then the measurement will reflect the phase noise of the spectrum analyser source as opposed to the signal generator. The only phase noise specifications for the spectrum analyser available was that the phase noise was -95dBc/Hz at an offset frequency of 30kHz. Therefore, the phase noise of the PLL can only be measured to about 30kHz and this figure is less than that of the phase noise from the simulation of the PLL.

From these spectrum measurements, the Allan variance and integrated phase noise values were determined for direct numerical comparison with values obtained from theory.

5.6.2 Synthesizer Phase Noise Measurements

This section presents the results of the phase noise measurements of the synthesizers. Figures 5.12, 5.13 and 5.14 show frequency spectrums of the synthesizer carrier at 200MHz. Using the technique described in the previous section and the results in Chapter 3, Table 5.4 was constructed. This shows the measured results at various offset frequencies above 10kHz.

Table 5.4: Phase Noise Measurements at $f_c = 200$MHz

f_m	Predicted $\mathcal{L}(f_m)$	Measured $\mathcal{L}(f_m)$
10 kHz	-97 dBc	-93 dBc
20 kHz	-95 dBc	-86 dBc
40 kHz	-95 dBc	-84 dBc
60 kHz	-98 dBc	-89 dBc
80 kHz	-102 dBc	-92 dBc
100 kHz	-103 dBc	-93 dBc
1 MHz	-125 dBc	-104 dBc

Similarly, Figures 5.15, 5.16 and 5.17 show frequency spectrums of the synthesizer carrier at 1590MHz and Table 5.5 shows phase noise predictions and1 measurement results. The cumulative phase noise for these measurements is 2.2 degrees for the frequency range of 10kHz to 100kHz. The predicted value fro n the simulation is 0.36 degrees for the same offset frequency band and is 1.9 degrees integrated over 10Hz to 100kHz.

Table 5.5: Phase Noise Measurements at $f_c = 1590$MHz

f_m	Predicted $\mathcal{L}(f_m)$	Measured $\mathcal{L}(f_m)$
10 kHz	-94 dBc	-82 dBc
20 kHz	-94 dBc	-72 dBc
40 kHz	-95 dBc	-84 dBc
60 kHz	-97 dBc	-89 dBc
80 kHz	-102 dBc	-92 dBc
100 kHz	-103 dBc	-93 dBc
1 MHz	-125 dBc	-101 dBc

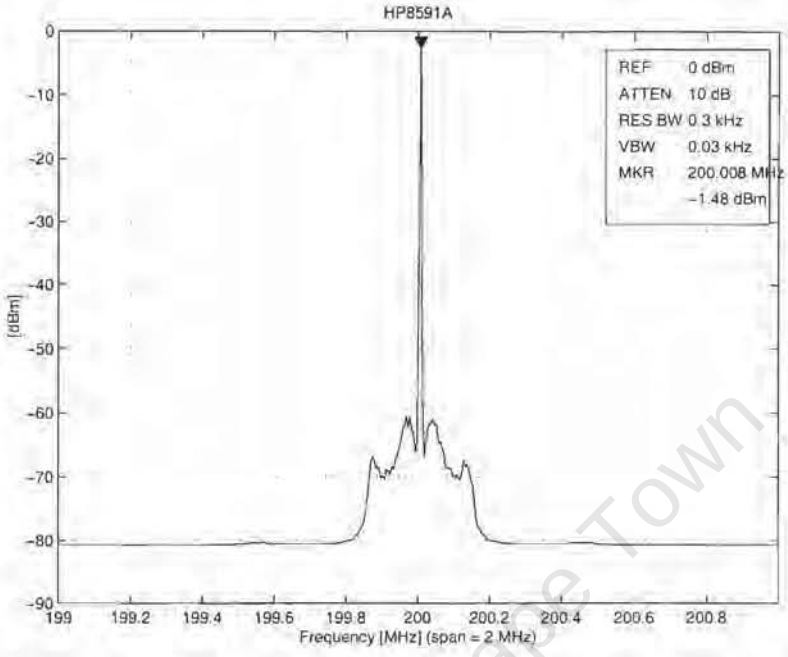

Figure 5.12: Synthesizer Spectrum, $f_c = 200$MHz, Span $= 2$MHz

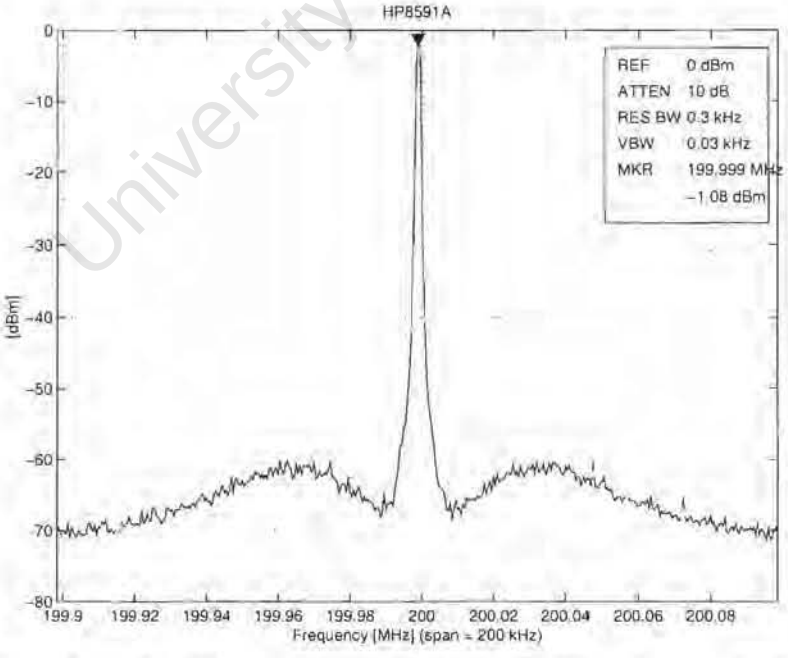

Figure 5.13: Synthesizer Spectrum, $f_c = 200$MHz, Span $= 200$kHz

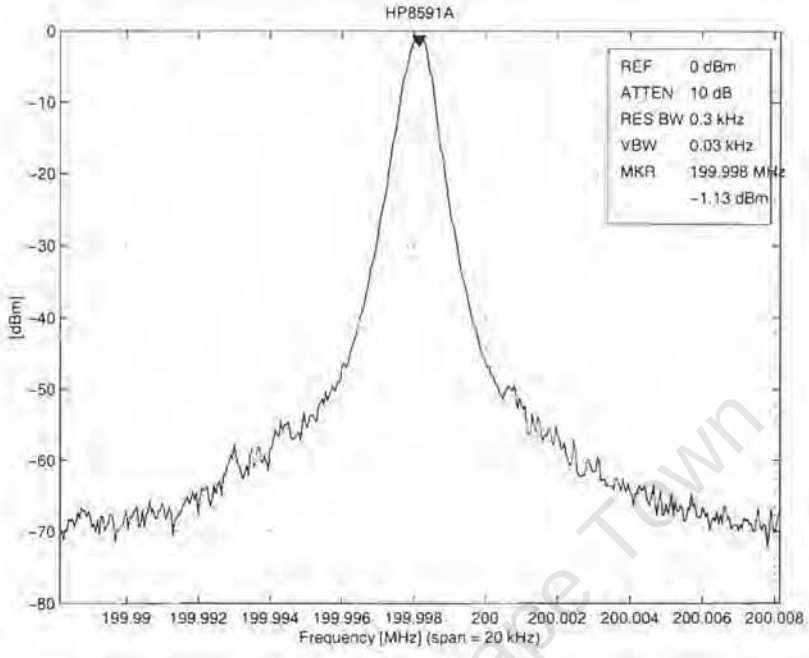

Figure 5.14: Synthesizer Spectrum, $f_c = 200$MHz, Span = 20kHz

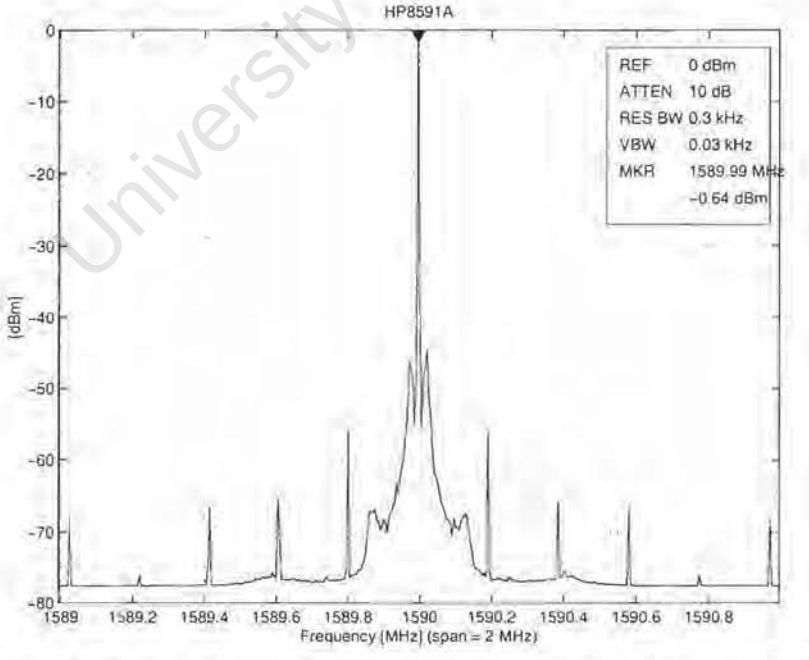

Figure 5.15: Synthesizer Spectrum, $f_c = 1590$MHz, Span = 2MHz

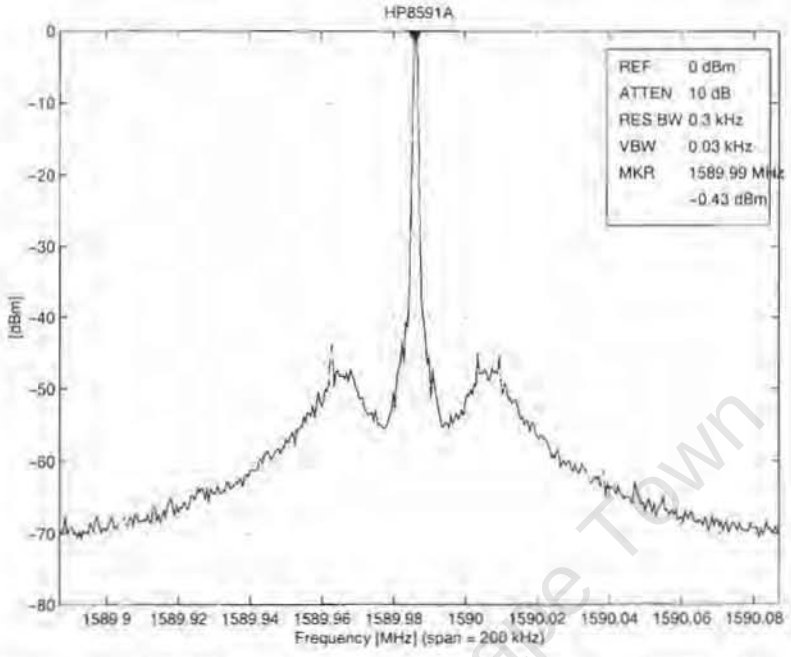

Figure 5.16: Synthesizer Spectrum, f_c = 1590MHz, Span = 200kHz

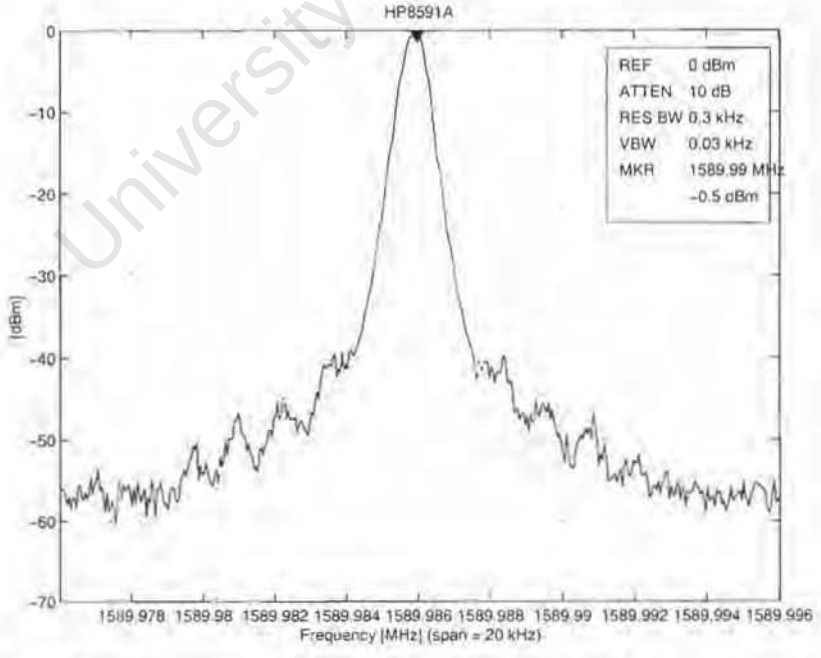

Figure 5.17: Synthesizer Spectrum, f_c = 1590MHz, Span = 20kHz

5.7 Synthesizer Lock Time

An HP54645D digital oscilloscope was used to record the synthesizer lock times. The control voltage of the voltage controlled oscillators was measured to obtain an estimate of the lock time. The lock time was measured for a single typical step of 10MHz and for a frequency band switch step. A frequency band switch step occurs when the variable prescalers change their divide ratio. When this occurs in a linear sweep through the frequency band, the phase locked loop changes from the maximum VCO output to the minimum. This change requires a longer settling time and therefore will be the maximum lock time experienced by the system.

Each of the control voltage measurements were made using the scope in AC coupling mode. The absolute voltages do not therefore reflect the actual control voltages. However, voltage differences are preserved.

Figures 5.18 and 5.19 show the control voltages for synthesizer steps from 200-210MHz and 1580-1590MHz respectively. The lock times are approximately 80μs and 100μs. The difference in lock times is expected as the synthesizer loop filter characteristics change as the value of the feedback divide ratio changes.

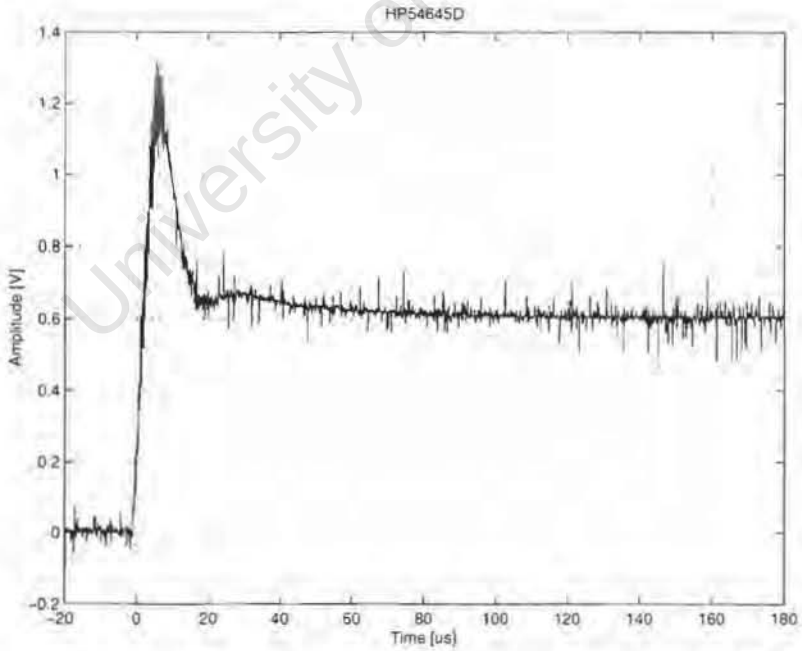

Figure 5.18: Synthesizer VCO Control Voltage, 200MHz to 210MHz

Figure 5.20 shows the control voltage for a step from 390MHz to 400MHz. The VCO output will jump from 1560MHz to 800MHz. Hence the control

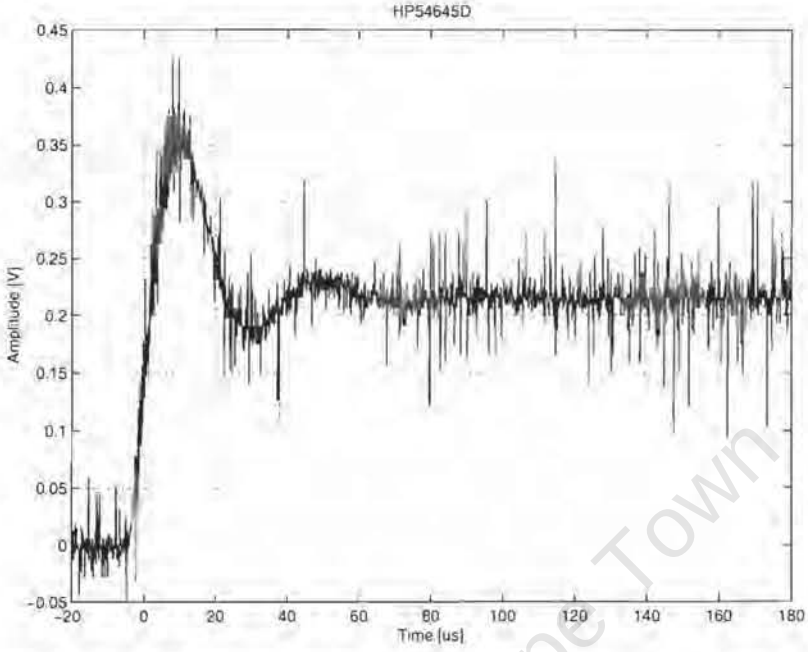

Figure 5.19: Synthesizer VCO Control Voltage, 1580MHz to 1590MHz

voltage is a negative jump. The lock time for this step is about 200μs which is almost double the 10MHz step time. The maximum lock time results from a negative frequency step from 800MHz to 790MHz. This can be seen in Figure 5.21 where the lock time is approximately 250μs.

The number of frequency scans per second is calculated from both measuring the lock time of the synthesizers and the data capture time. The data capture time is comprised of the ADC capture time and the time required by the microcontroller to store and transmit the samples to the HMI. The synthesizer lock time was taken as 200μs, the FPGA and microcontroller acquisition time measured as, 830.3μs. Therefore, for 140 frequency steps, the total data capture time is 144.2ms. The data transmission time, 97.2ms at 115200bps for 140 frequency steps. Therefore the total pulse repetition interval is 241.4ms. This means that the maximum number of scans per second is 4.

5.8 Transceiver Current Consumption

The current consumption for each of the modules was measured separately by measuring the current drawn from an external power supply unit and subtracting the consumption of the radar PSU module. This method will

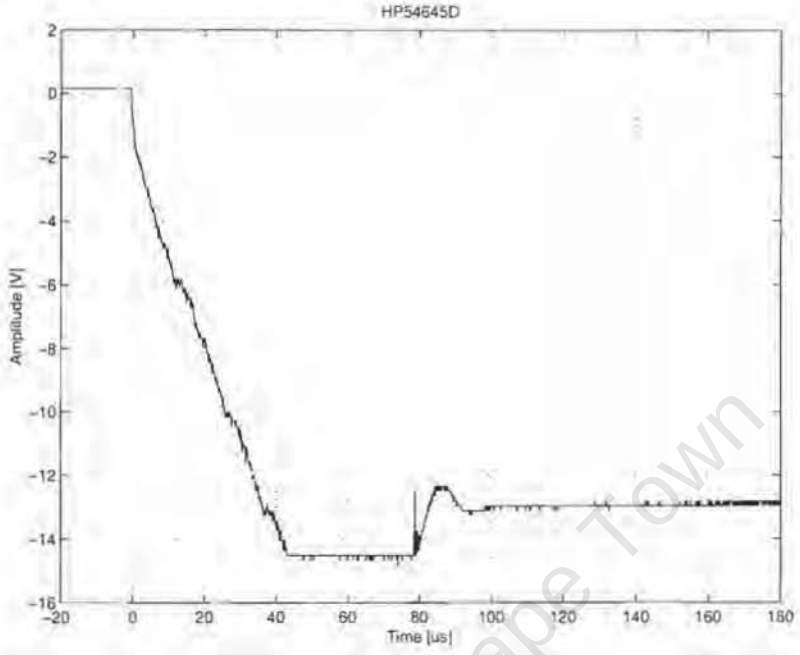

Figure 5.20: Synthesizer VCO Control Voltage, 390MHz to 100MHz

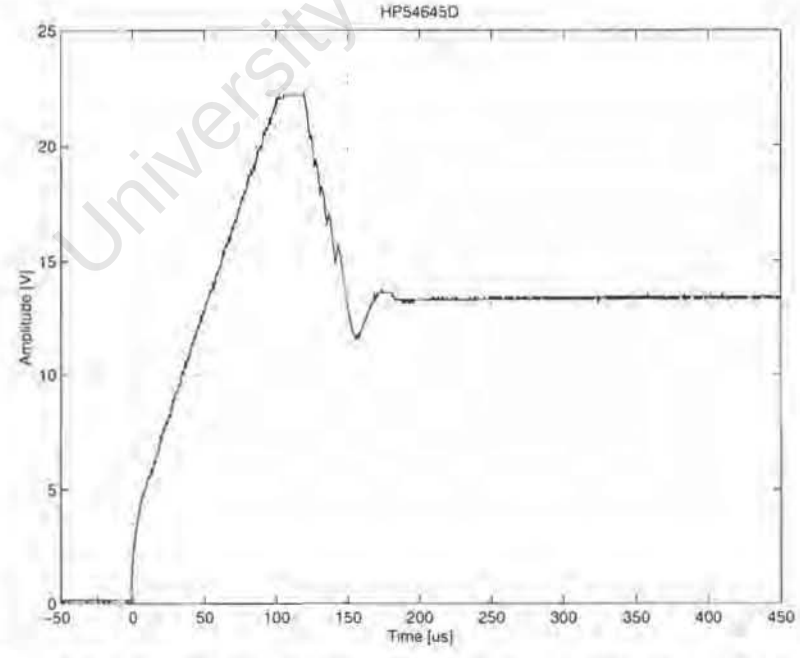

Figure 5.21: Synthesizer VCO Control Voltage, 800MHz to 790MHz

not produce accurate consumption results when the radar is operating, as there will be an increase in current when modules are connected together. However, it does provide a rough guide to the amount of current drawn by the radar for each of the modules. A more accurate measurement for the current drawn by the radar was made by measuring the current drawn with all of the modules connected together. These values are tabulated in Table 5.6 and can be compared to the values predicted in Table 4.5.

The total value of the measured does not sum to the sum of the measured values for each of the modules due to the measurement technique. Also, the total transceiver measured value was measured without the RCDC unit connected. This would draw some current from the transceiver and therefore increase the current consumption.

Table 5.6: Measured Transceiver Current Consumption [mA]

Module	Predicted (Table 4.5)	Measured
RFMB	120	34
REF	90	27
TXS	306.2	142
LOS	306.2	160
RFIF	165	147
RFX	135	124
Total	**1122.4**	**714**

5.9 Specifications Comparison

This section presents a comparison of the system specifications with the design implementation predictions and measured values. The comparison is shown in Table 5.7.

Table 5.7: Design Summary

Parameter	Specification	Design/Implementation	Measured
Dynamic Range	> 70dB	51.1dB (Section 3.2.2)	47dB to 57dB (Section 5.4)
Frequency Scans per Second	> 10	9 (Section 3.2.4)	4 (Section 5.7)
Current Consumption	< 2A	1122.4 (Table 4.5)	714mA (Table 5.6)
Harmonics (inside IF bandwidth) (outside IF bandwidth)	 < -80dBc < -3dBc	Unspecified	 Not measured -17dBc (Figure 5.6)
RMS Cumulative Phase Noise	< 0.2°	1.9° (10Hz - 100kHz) (Section 3.2.2)	2.2° (10kHz - 100kHz) (Section 5.6.2)
Step Time	< 62μs	120μs (Section 3.2.4)	200μs (Section 5.7)
TX Output Power	-15dBm to +15dBm	-8dBm to +15dBm, (Figures 4.3, 4.5 and 4.6)	-3dBm to +14dBm (Table 5.3)
Maximum RF Input	-25dBm	-28dBm (Figure 4.5)	Not measured

Chapter 6

Summary

A 200 to 1600MHz, stepped frequency, ground penetrating radar transceiver was designed and constructed. The performance of the transceiver was measured and presented in Table 5.7 against the system specifications and the predictions from the design and implementation calculations. This chapter discusses the comparisons showing where the measurements meet the specifications and presents reasons for differences, where they differ. From this discussion, conclusions about the success of the project are drawn and recommendations for future improvements are made.

6.1 Discussion of Transceiver Measurements

The dynamic range of the receiver was measured to be greater than 47dB but less than 57dB. This is in the region of the predicted value of 51.1dB. The upper bound of the measured value is greater than that of the value predicted from the theory. This is possible, as the predicted value is does not consider the effect of sample averaging. However, two possibilities exist: either the averaging is improving the dynamic range or the phase noise of the synthesizer is better than the predicted value.

The synthesizer cumulative phase noise was calculated from the phase noise measurements. However, these measurements were only made over an offset frequency band of 10KHz to 1MHz. The cumulative phase noise over this region was calculated to be 2.2 degrees which was more than the 0.36 degrees predicted by the simulation. This was due to a 22dB difference between the predicted and measured phase noise value at 20kHz from the offset frequency. This difference could be due to factors not simulated, such as power supply noise, or inaccurate phase noise measurements due to the

equipment available. However, if we assume that the phase noise values of the synthesizer are good approximations of the simulated values in the loop bandwidth of the phase locked loop, and the measured values are good approximations outside the loop bandwidth, then combining these, the cumulated phase noise is calculated to be 2.9 degrees. This is comparable to the 1.9 degrees, integrated from 10Hz to 100kHz which is predicted by the simulation. Therefore, as the phase noise is not accurately known, there is insufficient data to conclude the cause of the discrepancy in the dynamic range.

The highest frequency harmonics outside the IF bandwidth were lower than the specification value of -3dBm. The highest harmonics measured were -17dB below the carrier. The harmonics in the IF bandwidth were unable to be directly measured, due as the controller software to defaulted the reference channel when idle to save power. However, the harmonics that would mix into the IF bandwidth are the phase locked loop reference spurs. These were measured to be -55dB below the carrier. The predicted value from the simulation was -57dBc. Assuming the maximum received signal of -28dBm, the input to the mixer is +1dBm. The reference spurs will then be at -54dBm. These will then be mixed into the IF band by the local oscillator reference spurs at -48dBm. It is therefore predicted that the current reference spur levels are small enough so that they will not affect the radar data. Figure 5.11 shows the reference spurs at -55dBm. Also present are spurious signals closer to the carrier. These can be better seen in Figure 5.15. These signals are 190kHz from the carrier signal. It is unlikely that these could have been caused by the power supply module of the radar. as the DC/DC converters were specified to operate at 100kHz and 400kHz and these is no harmonic at 100kHz from the carrier. The source of these spurious signal is not known. Like the reference sidebands, these signals would probably be too low to corrupt the radar data.

The number of frequency scans per minute was less than that specified as the amount of data transmitted from the radar to the HMI was doubled with the addition of the reference channel. The number of frequency scans per second was calculated from measurements to be 4 as opposed to the specification requirement of 10.

The step time of the synthesizers and the current consumption measured values were less than or equal to the specification values. The specified transmitted power range of -15dBm to +15dBm was not achieved. The measured output power range was -3dBm to +14dBm.

Figure 5.2 shows raw received radar data and was used to illustrated the phase errors due to the synthesizer band switching. It also shows that for the higher transmitted frequencies, the received data is very much larger in

amplitude than the lower frequencies, despite the equal transmitted output power for each frequency. This reduces the dynamic range of the radar, as at the higher frequencies, the signal saturates sooner. The ratio of the maximum to minimum data amplitudes is approximately 20, which means that 20dB of dynamic range is being lost. No reason was found for this phenomenon. However, if this is the case, then the system specification of 70dB dynamic range would be achieved.

6.2 Conclusions

Based on the results presented in this dissertation, the following conclusions are be drawn:

- A stepped frequency, ground penetrating radar transceiver module was designed and constructed and found to operate with the radar.
- There was an insufficient accuracy in phase noise measurements to characterise the causes for the transceiver limitations completely.
- There were unexplained spurious harmonics close to the carrier signal at high frequencies.
- Most of the system specifications were achieved with the exception of the dynamic range, synthesizer phase noise and number of frequency scan per second.
- The transceiver dynamic range performance can be improved by limiting the frequency band to less than 800MHz.

6.3 Recommendations

Based on the conclusions, the following recommendations are made:

- Accurate measurements of the phase noise need to made.
- IF harmonic levels need to be simulated and investigated to ensure that they do not significantly affect the radar data.
- The radar should be used temporarily over a reduced bandwidth to improve the dynamic range.

Appendix A

Stepped Frequency and Ground Penetrating Radar

This appendix briefly reviews the principles of stepped frequency radar and ground penetrating radar. Relevant equations are presented for use in the design of the radar. The appendix concludes with the results of a simple stepped frequency simulation to illustrate the data obtained from the radar.

A.1 Stepped Frequency Radar

Stepped frequency radar is one of several radar waveforms developed to overcome the power bandwidth limitations of pulse radars. This is achieved by the transmission of a high mean power over a longer waveform which extends the range capability of the radar yet retains a wide bandwidth for high resolutions. Stepped frequency radar techniques for the detection of subsurface objects have been investigated since about 1979 [13]. The following sections briefly describe the principles of stepped frequency radar and the equations relating to this technique. Detailed descriptions of stepped frequency radar can be found in [14, 30, 10, 37, 21].

A.1.1 Stepped Frequency Radar Operation

Stepped frequency radar determines the distance to targets by constructing a synthetic range profile in the spatial time domain. The synthetic range profile is a time domain approximation of the frequency response of a combination of the medium through which the electromagnetic radiation propagates, and any targets or dielectric interfaces present in the beamwidth of the

radar. It is constructed by sequentially transmitting a series of n frequencies, $f_i = f_0 + i\Delta f$ where $0 \leq i \leq n-1$ and for each measuring the amplitude and phase shift of the received signal with respect to the transmitted signal. Figure A.1 shows the time domain characteristic of the transmitted waveform for a stepped frequency radar where T is known as the pulse repetition time of the radar and t_d is the sum of the data capture time and data transmission time.

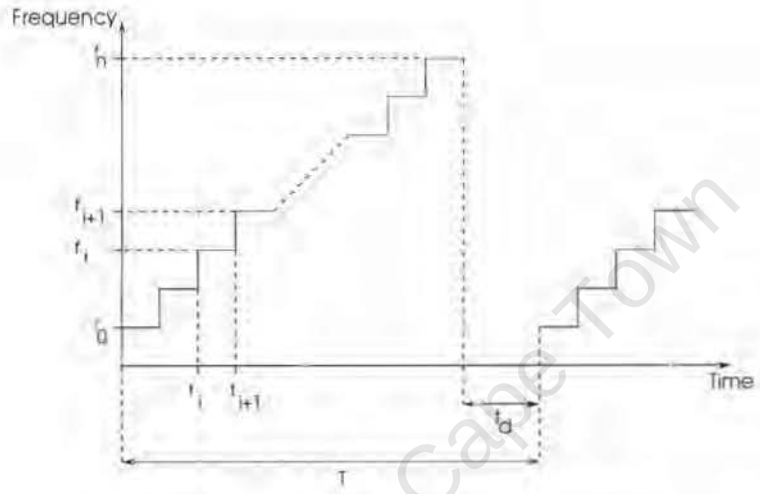

Figure A.1: Stepped Frequency Waveform

The phase shift in the received signal is a proportional to the transmitted frequency and the range to the target. This is shown in Equation A.1 for a point target stationary relative to the radar.

$$\phi_i = -2\pi f_i \left(\frac{2R}{c}\right) \tag{A.1}$$

For a single target at constant range, R, there will be a linear change in phase for each frequency step. This is shown in Figure A.2(c). The real and imaginary parts of the data will therefore be sinusoidal with a frequency corresponding to the phase unwrapping rate. This can be seen in Figures A.2(a) and A.2(b). Targets closer and further away will produce respectively lower and higher phase unwrapping rates. For more than one target, the return will be a vector addition of the returns from each of the targets. The IDFT, or FFT equivalent, can then be used to approximately separate signal returns from targets at different ranges by using the different phase unwrapping rates to create the synthetic range profile in the spatial time domain. Examples of the synthetic range profiles are shown in Figures A.2(d) and A.3(d).

Wehner [37] shows that the IFFT approximation to synthetic range profile

for a particular radar azimuth position is given by

$$\vec{\mathbf{H}} = \sum_{l=0}^{n-1} e^{-j2\pi f_0 \frac{2R}{c}} \frac{\sin(\pi\chi)}{\sin\left(\frac{\pi\chi}{n}\right)} e^{j\frac{n-1}{2}\frac{2\pi\chi}{n}} \tag{A.2}$$

where $\chi = -2nR\Delta f/c + l$ and l is the range bin in which synthetic range profile value, H_l occurs, $0 \leq l \leq n-1$. The peak value of the magnitude of the synthetic range profile is equal to n.

Examples of stepped frequency data are shown in Figures A.2 and A.3 produced from a simulation of SF radar. The simulation used a bandwidth of 1390MHz (200MHz to 1590MHz) with 139 frequency steps (140 frequencies). The first plot shows a single target at 0.7 meters from the radar. The second, two targets, 0.7 and 3.1 meters from the radar respectively. Plots (a) and (b) of each figure show the real and imaginary parts of the spatial frequency domain data. Plot (c) shows the phase of the spatial frequency domain data and plot (d) the synthetic range profile.

A.2 Ground Penetrating Radar

Ground penetrating radar relies on several factors for target detection:

(*i*) efficient coupling of electromagnetic radiation into the ground;

(*ii*) adequate penetration of the radiation through the ground with regard to target depth;

(*iii*) obtaining from buried objects or other dielectric discontinuities a sufficiently large back scattered signal for detection at the ground surface.

This section will present an overview of the equations used to determine the performance of ground penetrating radar, based on the requirements mentioned above.

A.2.1 Propagation of Electromagnetic Waves

The propagation of a uniform plane electromagnetic wave, polarized in the x-plane through an isotropic, linear medium in a single direction, z, is described by the phasor solution (given in Equation A.3) to the one-dimensional Helmholtz equation.

$$E_x(z) = E_0 e^{-jkz} \tag{A.3}$$

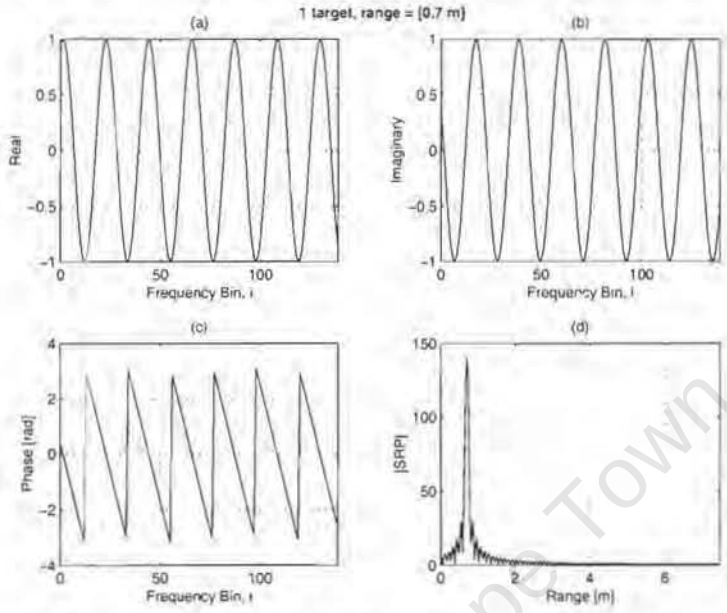

Figure A.2: SF Radar Simulation (single target)

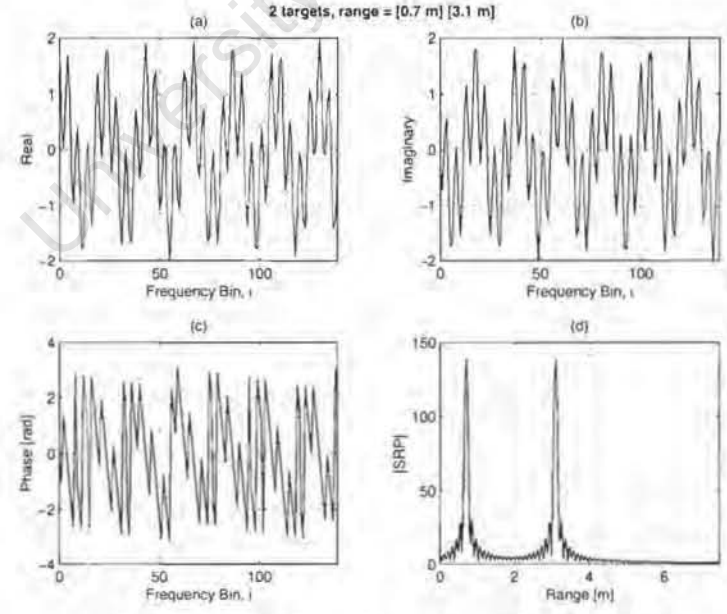

Figure A.3: SF Radar Simulation (two targets)

E_0 is an electric field constant and k is the propagation constant which gives the change in amplitude and phase per unit length of the plane wave. For dielectric materials with real permeability and complex permittivity we have $k = \omega\sqrt{\mu(\varepsilon' - j\varepsilon'')}$ where the conduction currents are included in the loss factor ε''.

The propagation constant, k, can be split into a real, α, and an imaginary, β, part. α is known as the attenuation constant and β the phase constant. These can be approximated by [21]

$$\alpha \approx 188.5\frac{\sigma}{\sqrt{\varepsilon_{r(g)}}} \text{ [Np/m]} \tag{A.4}$$

$$\beta \approx \omega\sqrt{\mu\varepsilon} \text{ [rad/m]} \tag{A.5}$$

The phase velocity of an electromagnetic wave depends on the relative permittivity and permeability of the medium. The phase velocity in a medium with relative permittivity, $\varepsilon_{r(g)}$, and relative permeability, $\mu_{r(g)}$, is given by

$$v = \frac{c}{\sqrt{\mu_{r(g)}\varepsilon_{r(g)}}} \text{ [m/s]} \tag{A.6}$$

A.2.2 Ground Electromagnetic Characteristics

For subsurface radar, the medium in which targets exist and through which electromagnetic radiation propagates is the the ground. The ground is in general a heterogeneous medium making it very difficult to predict accurately the response to an electromagnetic wave. However, some very general assumptions can be made. It is observed that materials that make up the soil near the surface have the following general characteristics [7]: the attenuation constant, α, rises with increasing frequency and is higher in wet conditions than dry ones. Table A.1 has been extracted from references and gives some examples of the one-way attenuation in dBm^{-1} for different frequencies and ground types. These attenuations are merely a rough guide, but do provide a first order approximation. Much work has been spent on different medium models which have been summarised in [7].

In general, for non-magnetic media, the permeability of the ground is equal to the permeability of free space, μ_0, which is approximately $4\pi \times 10^{-7}$. The permittivity, however, is not always easy to determine as the ground is a heterogeneous environment. Much of the work carried out in this field has again been summarised in [7]. Table A.2 shows some relative permittivities for different mediums.

Table A.1: One-Way Attenuation [dBm^{-1}]

Medium	Frequency	
	100 MHz	1 GHz
Wet Clay	20-30	100
Loamy Soil	-	20-30
Sandy Soil	-	10
Dry Desert Sand	-	1
Sea Water	200	300
Fresh Water	4	40

Table A.2: Relative Permittivities

Medium	Relative Permittivity ($\varepsilon_{r(g)}$)
Solid constituents of soils	2-6
Soil	4-40
Water	80

A.2.3 Ground Penetrating Radar Target Characteristics

The target radar cross section is a measure of the proportion of the incident signal reflected back to the radar by the target, and is dependent on the shape and physical size of the target and the material from which the target is comprised. It is difficult to predict the radar cross section of targets other than simple geometric shapes, thus making it difficult to model accurately the performance of ground penetrating radar.

A.2.4 Antenna Radiation Fields

The radiation field surrounding an antenna is usually divided into three regions which are the reactive near-field, the radiating near-field (Fresnel) and the far-field (Fraunhofer) regions [3]. These regions are defined by the approximate field structure in each. Most radar analysis uses the far field approximation in determining system performance. However, the targets in ground penetrating radar are generally close to the antennas and fall in the near field.

[3] states that the far field region exists at distances greater than $R > 2D^2/\lambda$ where D is the largest dimension of the antenna. Thus an antenna with $D =$

30cm and operating at 900MHz in free space ($\lambda = 0.33$m), the far field region start at about 0.54 meters from the antenna. Therefore targets just beneath the surface of the radar will appear in the reactive and radiating near-field regions. The effect of this will not be discussed in this dissertation, and the performance of the radar will be predicted using a far-field assumption. However, it must be noted that the results presented are made with this assumption.

A.3 Range Resolution

Range resolution, also referred to as the depth resolution in subsurface radar, depends on the bandwidth of the received signal. This is given by Equation A.7 where v_g is the velocity of the electromagnetic signal in the ground.

$$\delta R = \frac{v_g}{2n\Delta f} \tag{A.7}$$

Two objects closer than this distance will not be able to be resolved as separate targets by the radar.

Appendix B

Frequency Instability Definitions

Work carried out in the latter half of the 1960's and the 1970's defined the modern methods for specifying frequency stability [2, 5, 29]. This appendix uses presents a brief review of that work to define the parameters used in this dissertation to characterise the frequency synthesizers.

A frequency instability measurement is a value that specifies the extend to which a frequency source changes from its prescribed value over a period of time. Frequency instability is caused by the oscillator component noise, temperature drift and oscillator aging. Temperature drift and aging are forms of long term frequency instability and are measured in units such as part per million per degree of temperature change or per day or year and are usually specified by the manufacturer of the oscillator. However, a stepped frequency radar pulse is sampled over a time period of the order of tens of microseconds. The frequency drift over this time will be due predominantly to the oscillator noise and not temperature drift and aging. It must be noted that for a change in temperature, measurements from the radar would have a corresponding change. Frequency instability due to oscillator component noise is known as short term frequency instability. This will now be defined.

A sinusoid of frequency, ν_0 and with time varying amplitude noise, $a_n(t)$ and phase noise, $\phi_n(t)$ can be represented by

$$s(t) = [A_0 + a(t)] \cos[2\pi\nu_0 t + \phi(t)] \tag{B.1}$$

The instantaneous angular frequency of this signal is the time derivative of the total oscillator phase, $\theta(t)$. Thus,

$$\omega(t) = \frac{d\theta(t)}{dt} = \frac{d}{dt}[2\pi\nu_0 t + \phi(t)] \tag{B.2}$$

and the instantaneous frequency is

$$\nu(t) = \nu_0 + \frac{1}{2\pi}\frac{d\phi(t)}{dt} \tag{B.3}$$

This is used to define the fractional frequency, $y(y)$

$$y(t) = \frac{\nu(t) - \nu_0}{\nu_0} = \frac{1}{2\pi\nu_0}\frac{d\phi(t)}{dt} \tag{B.4}$$

The spectral density $S_\phi(f)$ of the phase fluctuations $\phi(t)$ is a measure of relative modulation of the signal at a frequency offset from the carrier by f hertz. This is usually measured in radians squared per hertz [rad^2/Hz] or decibels relative to the carrier [dBc]. This can be simply related to the spectral density $S_y(f)$ of the instantaneous fractional frequency fluctuations $y(t)$ by

$$S_\phi(f) = \left(\frac{\nu_0}{f}\right)^2 S_y(f) \tag{B.5}$$

A similar measurement to the spectral density of the phase fluctuations and what is usually quoted by manufactures is the one-sided power spectral density of the phase fluctuations, $\mathcal{L}(f)$. This is the relative power spectral density of phase noise in watts per hertz per watt of carrier power as a function of positive offset frequency f from the carrier.

The cumulative phase, $\phi_c(t)$ is defined as the phase change between the phase of a signal at time t and $t+\tau$. Therefore

$$\phi_c(t) = \theta(t+\tau) - \theta(t) = 2\pi\int_t^{t+\tau}\nu(\xi)\,d\xi \tag{B.6}$$

$\phi_c(t)$ will be a random process based on the statistics of the frequency fluctuations. Assuming wide-sense stationary and ergodic statistics, [37] provides a conversion from the one-sided density $\mathcal{L}(f)$ to the variance of the cumulative phase fluctuations for a time difference τ. This integral tends to a limit for integration beyond $f = 1/\tau$.

$$\phi_c^2 = 8\int_0^\infty \mathcal{L}(f)\sin^2(\pi f\tau)\,df \tag{B.7}$$

A widely used time domain measurement of frequency instability is the Allan variance $\sigma_y^2(\tau)$. This is defined as

$$\sigma_y^2(\tau) = \left\langle \frac{1}{2}(\bar{y}_{k+1} - \bar{y}_k)^2 \right\rangle \tag{B.8}$$

where $\bar{y}_{k+1}$ and $\bar{y}_k$ are two samples of the average fractional frequency separated by a time interval τ. The average fractional frequency is

$$\bar{y}_k = \int_{t_k}^{t_k+\tau} y(t)\,dt \tag{B.9}$$

Using Equation B.5 the Allan variance can be computed from the spectral density of phase fluctuations $S_\varphi(f)$ [9].

$$\sigma_y^2(\tau) = \frac{2}{(\pi\nu_0\tau)^2}\int_0^\infty S_\phi(f)\sin^4(\pi f\tau)\,df \tag{B.10}$$

The root mean squared cumulative phase can be calculated from the the Allan variance.

$$\sigma_c = 2\pi\tau\sigma_y\nu_0 \tag{B.11}$$

Appendix C

Phase Locked Loop Simulation Model

This appendix will present the theory and model used to obtain the simulation results for the phase locked loop. It will start with the model used to describe the phase locked loop. This will be followed by a description of the noise sources in the loop and their contribution to the phase noise.

C.1 Phase Locked Loop Model

In a theoretical prediction of frequency instability for a phase locked loop frequency synthesizer, it is easier to predict the frequency domain phase noise plot of the synthesizer. Figure C.1 shows how the noise contributions in the phase locked loop are modeled to predict the total phase noise of the loop. The noise contributions from the reference oscillator, the voltage controlled oscillator and the loop filter have been included in the model. The model could be further improved with the noise from the phase detector being included, but this is usually a very small contribution.

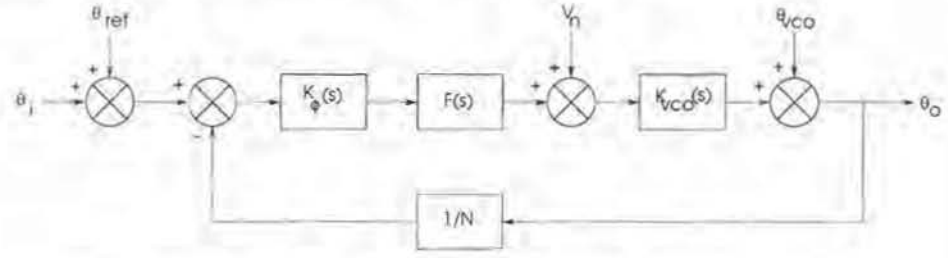

Figure C.1: Block Diagram of PLL Noise Contributions

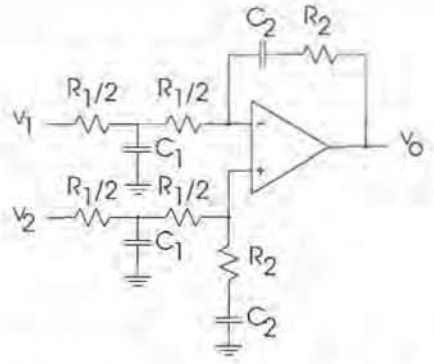

Figure C.2: Loop Filter Circuit Diagram

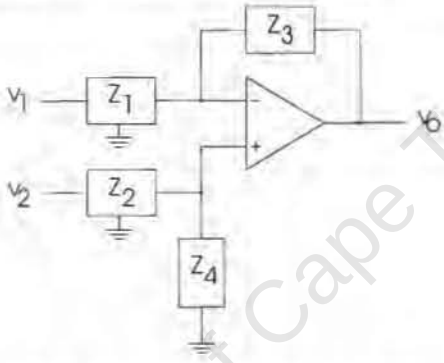

Figure C.3: Loop Filter Equivalent Structure

C.1.1 Phase Detector

$$K_\phi(s) = K_\phi e^{-\frac{s}{2f_\phi}} \tag{C.1}$$

C.1.2 Loop Filter

The circuit diagram of the loop filter is shown in Figure C.2. This circuit is of the form shown in Figure C.3. For a differential amplifier of this form, if $Z_3/Z_1 = Z_4/Z_2$ then $V_o/(V_2 - V_1) = Z_3/Z_1$. The components that comprise the impedance Z_1 form a 3-terminal network. [34] provides a method for computing Z_3/Z_1 using Y-parameters. Y_f and Y_i are the short circuit forward admittances for the feedback and the input networks respectively. These are shown in Figure C.4. The filter transfer function is then $-Y_{ti}/Y_{tf}$. From Appendix VI of [34]

$$Y_i = \frac{-1}{R_1\left(1 + s\frac{R_1^2 C_1}{4R_1}\right)}$$

$$= \frac{-1}{R_1\left(1+s\frac{R_1C_1}{4}\right)}$$

and

$$Y_f = -\frac{sC_2}{1+sR_2C_2}$$

From this the filter transfer function is

$$\begin{aligned}\frac{V_o}{V_i} &= -\frac{Y_i}{Y_f} \\ &= -\frac{1+sR_2C_2}{sR_1C_2\left(1+s\frac{R_1C_1}{4}\right)} \\ &= -\frac{1+sT_2}{sT_1\left(1+sT_3\right)}\end{aligned}$$

where $T_1 = R_1C_2$, $T_2 = R_2C_2$ and $T_3 = R_1C_1/4$.

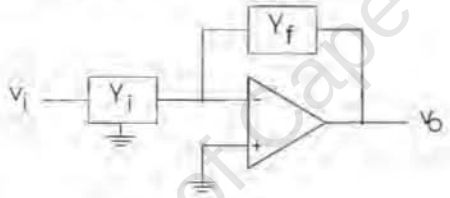

Figure C.4: Loop Filter Equivalent Structure

C.1.3 Voltage Controlled Oscillator

$$K_{vco}(s) = \frac{K_{vco}}{s} \tag{C.2}$$

C.1.4 Phase Locked Loop Transfer Functions

$$\frac{\theta_o}{\theta_i} = \frac{K(s)F(s)}{R\left(1+\frac{1}{N}K(s)F(s)\right)} \tag{C.3}$$

where $K(s) = K_{phi}(s)K_{vco}(s)$.

$$\frac{\theta_o}{\theta_{vco}} = \frac{1}{1+\frac{1}{N}K(s)F(s)} \tag{C.4}$$

$$\frac{\theta_o}{V_n} = \frac{K_{vco}(s)}{1+\frac{1}{N}K(s)F(s)} \tag{C.5}$$

C.2 Noise Sources

C.2.1 Loop Filter

The resistors and operational amplifier of the loop filter produce noise on the control signal of the voltage controlled oscillator which modulates the output adding to the total phase noise of the synthesizer. The filter noise sources are shown in Figure C.5. The total output noise voltage density may be

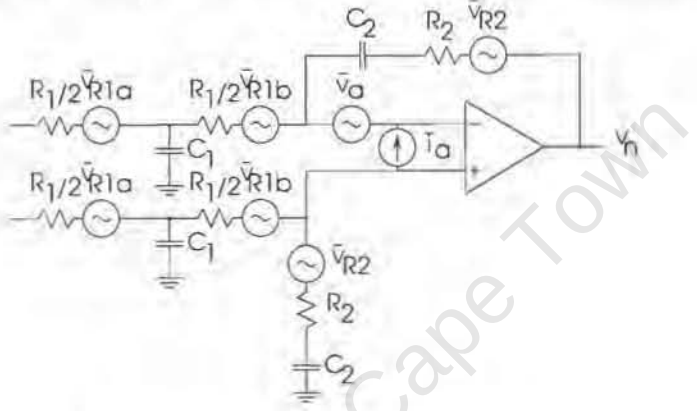

Figure C.5: Loop Filter Noise Model

found by finding the output noise due to each noise source and then using the principle of superposition. However, because the sources are random noise and are uncorrelated, the mean square voltages (power) are additive, not the individual noise voltages. The output noise voltage densities due to each source are found from op amp theory and given in Equations C.8 to C.14.

$$v_n\left(v_{\bar{R}1a}\right) = 4kT\frac{R_1}{2}\frac{Z_f}{Z_i} \tag{C.6}$$

$$= 4kT\frac{R_1}{2}\frac{sT_2+1}{sT_1\left(sT_3+1\right)} \tag{C.7}$$

$$v_n\left(v_{\bar{R}1b}\right) = 4kT\frac{R_1}{2}\frac{V_o}{V_i}\frac{V_i}{V_{C_1}} \tag{C.8}$$

$$= 4kT\frac{R_1}{2}\frac{\left(s2T_3+1\right)\left(sT_2+1\right)}{sT_1\left(sT_3+1\right)} \tag{C.9}$$

$$v_n\left(v_{\bar{R}2}\right) = 4kTR_2 \tag{C.10}$$

$$v_n\left(\bar{v_a}\right) = \bar{v_a}\left(\frac{Z_i+Z_f}{Z_i}\right) \tag{C.11}$$

$$= \bar{v_a}\frac{sT_1\left(1+sT_3\right)+\left(1+sT_2\right)\left(1+s2T_3\right)}{sT_1\left(1+sT_3\right)} \tag{C.12}$$

$$v_n\left(\bar{i_a}\right) = \bar{i_a}Z_f \tag{C.13}$$

$$= \bar{i_a}\frac{1+sT_2}{sC_2} \tag{C.14}$$

The total output noise voltage density may be found as the square root of the sum of the squares of each contribution.

$$v_n = \sqrt{v_n\left(\bar{v_{R1a}}\right)^2 + v_n\left(\bar{v_{R1b}}\right)^2 + v_n\left(\bar{v_{R2}}\right)^2 + v_n\left(\bar{v_a}\right)^2 + v_n\left(\bar{i_a}\right)^2} \tag{C.15}$$

Appendix D

Acceptance Test Procedure

The acceptance test procedure (ATP) defines the procedure for testing the transceiver for correct operation. Each of the transceiver modules is systematically checked by testing of the parts of a module individually. For each test, the aim and method are described.

D.1 Transceiver Motherboard Test Procedure

Motherboard Power Test	
Aim	To ensure that each of the socket pins on the motherboard supply the correct voltage to the daughter-boards.
Method	Using a multimeter, check each of the voltages with the motherboard powered and ensure that they correspond to the expected voltage on the daughter-board.

D.2 Frequency Reference Test Procedure

Frequency Reference Power-On Test	
Aim	To ensure that the frequency reference board powers up with no short circuit faults.
Method	Using an external power source, apply the +5V to the board with the current limited initially to 0A. Slowly increase the current to no more than 110% of the specified current given in Table 4.5 in Chapter 4 (90mA). The current should roughly equal to the specified current and the voltage should not have dropped below +5V.

Frequency Reference Operational Test	
Aim	To ensure that the frequency reference board generates the required four frequencies of 8MHz, 4MHz, 2MHz and 2MHz.
Method	Apply power to the frequency reference board. Measure the signal generated by the temperature compensated crystal oscillator (TCXO). It should be a 16MHz square wave with a low of less than 0.4V and a high of greater than 4V. Measure the frequency of the output signal from each of the coaxial connectors. The frequencies generated should be 8MHz, 4MHz, 2MHz and 2MHz.

D.3 Synthesizer Test Procedure

Synthesizer Power-On Test	
Aim	To ensure that the synthesizer board powers up with no short circuit faults.
Method	Using an external power source, apply each of the required voltages (+5V, +9V, +24V and -5V) one by one to the synthesizer power sockets with the current limited initially to 0A. Slowly increase the current to no more than 110% of the specified currents given in Table 4.5 in Chapter 4. Each of the supply current should roughly equal the specified currents with no voltage drop from the preset value on the power supply.

Voltage Controlled Oscillator Test	
Aim	To ensure correct operation of the voltage controlled oscillator.
Method	Attach an manually variable voltage to the control input of the VCO. Sweep the voltage from 0V to 24V and observe the VCO frequency using a frequency counter or spectrum analyser.

Phase Locked Loop IC Test	
Aim	To ensure correct operation of the PLL IC.
Method	Attach an manually variable voltage to the control input of the VCO. Generate a 2MHz reference frequency signal for the PLL IC. Set the feedback divide ratio (N) to a known value between 400 and 800. Adjust the VCO control voltage to approximately the frequency that when divided by N, results in 2MHz. Monitor the PDU and PDD pins of the PLL IC on an oscilloscope. As the VCO frequency nears the required frequency, the pulses on the PDU and PDD lines should become increasingly narrow as described in Chapter 4.

Synthesizer Lock Test	
Aim	To ensure that the phase locked loop locks to the correct frequency.
Method	Using the Mercury-B radar software, set the output to 200MHz, 310MHz, 400MHz, 570MHz, 800MHz and 1320MHz. These frequencies cover all three synthesizer bands including the boundary frequencies. View the output of the synthesizer on a frequency counter or spectrum analyser.

Variable Attenuator Test	
Aim	To ensure correct operation of the variable attenuator.
Method	Connect a manually controllable voltage to the control input of the variable attenuator. Set the output frequency to 1600MHz. Adjust the voltage from 0V to -3V. The output power level of the synthesizer should change from approximately -25dBm (0V) to +11dBm (-3V) on a power meter or spectrum analyser.

Maximum/Minimum Output Power Test	
Aim	To measure the synthesizer output power variation obtainable across the band.
Method	Set the variable attenuator gain control value to 0. Set the TXS frequency to 200MHz, 400MHz, 800MHz and 1590MHz and for each, record the output power level. Set the variable attenuator value to maximum, and record the output power level for the same frequencies.

Constant Output Power Test	
Aim	To test that the output power level is able to be controlled to produce a constant level across the band of the synthesizer.
Method	Using the synthesizer attenuation calibration unit of the Mercury-B radar software, set the frequency sweep from 200MHz to 1590MHz over 3 seconds. Using the graphing functions, adjust the DAC values such that the frequency sweep produces an almost flat spectrum.

D.4 RF/IF Test Procedure

RF/IF Power-On Test	
Aim	To ensure that the RF/IF board powers up with no short circuit faults.
Method	Using an external power source, apply each of the required voltages (+5V, +9V and -5V) in turn to the RF/IF power sockets with the current initially limited to 0A. Slowly increase the current to no more than 110% of the specified current given in Table 4.5 in Chapter 4. Each of the supply currents should roughly equal the specified currents with no voltage drop from the preset value on the power supply.

Reference Channel Test	
Aim	To ensure that the reference channel is operating correctly.
Method	Set the transmit synthesizer to 800MHz at an output power level of -2dBm and the local oscillator synthesizer to 802MHz at -5dBm. Measure the signal at the IF port of the RFIF board. There should be a 2MHz signal with a power level of -25dBm or 36mV_{pp} into a 50Ω load.

Receive Channel Test	
Aim	To ensure that the receive channel is operating correctly.
Method	Set the transmit synthesizer to 800MHz at an output power level of -2dBm and the local oscillator synthesizer to 802MHz at -5dBm. A attach a cable from the transmit port to the receive port of the RFIF module. Measure the signal at the IF port of the RFIF board. There should be a 2MHz signal with a power level of 0dBm or 632mV_{pp} into a 50Ω load.

D.5 RFX Test Procedure

RFX TX Power-On Test	
Aim	To ensure that the RFX TX board powers up with no short circuit faults.
Method	Using an external power source, apply +9V to the RFX TX power sockets with the current limited initially to 0A. Slowly increase the current to no more than 110% of the specified current given in Table 4.5 in Chapter 4. The supply current should roughly equal the specified value at +9V.

RFX TX Operation Test	
Aim	To ensure that the RFX TX amplifier is operating correctly.
Method	Set the synthesizer to step from 200MHz to 1600MHz in 10MHz steps over a period of 2 seconds. Set the synthesizer level across the band to -3dBm. Use a spectrum analyser to view the signal and to hold the maximum value for each frequency. The output should be a constant amplitude frequency sweep at about +15dBm.

RFX TX Maximum/Minimum Power Level Test	
Aim	To measure the RFX TX maximum and minimum output power levels.
Method	Set the TXS output power to minimum. Record the RFX TX output power level for frequencies, 200MHz, 400MHz, 800MHz and 1590MHz. Set the TXS output power level to 0dBm and measure the RFX TX output power level for the same frequencies.

RFX RX Power-On Test	
Aim	To ensure that the RFX RX board powers up with no short circuit faults.
Method	Using an external power source, apply +9V to the RFX TX power sockets with the current limited initially to 0A. Slowly increase the current to no more than 110% of the specified current given in Table 4.5 in Chapter 4. The supply current should roughly equal the specified value at +9V.

RFX RX Operation Test	
Aim	To ensure that the RFX RX amplifier is operating correctly.
Method	Use an external frequency source to generate a stepped frequency signal from 200MHz to 1600MHz in 10MHz steps over a period of 2 seconds. Set the signal level across the band to -28dBm. Use a spectrum analyser to view the signal and to hold the maximum value for each frequency. The output should be a constant amplitude frequency sweep at about -7dBm.

Appendix E

Radar Measurements

The scope of this dissertation was only to describe the design and implementation of the transceiver module for the Mercury B ground penetrating radar. However, two measurements taken with the full GPR system are presented here. These are included in this document to show that the transceiver module worked with the rest of the radar.

The measurements are presented without interpretation. The first measurement, shown in Figure E.1, was taken outside along a road at the University of Cape Town. The second measurement, shown in Figure E.2 was taken inside a building, along a corridor on the sixth floor, at the University of Cape Town.

The major returns seen in Figure E.1 are believed to be from pipes buried under the scan area. Some of these pipes were identified by manhole covers on the road. The equally spaced returns from Figure E.2 are believed to be from the reinforcement bars in the concrete floor.

The depth scale on the images is not accurate as the ground permittivity was not accurately known. The radar data was processed using an average ground relative permittivity of 5. The radar frequency range used was 200MHz to 1200MHz as the antennas were designed to cover this frequency range. The range resolution was therefore 15cm. 100 frequency steps were used with a step size of 10MHz. The raw synthetic range profiles were upsampled by FFT interpolation to 512 samples in both the range and azimuth directions to produce the images. The raw radar data was inverted to the synthetic range profile using the FFT.

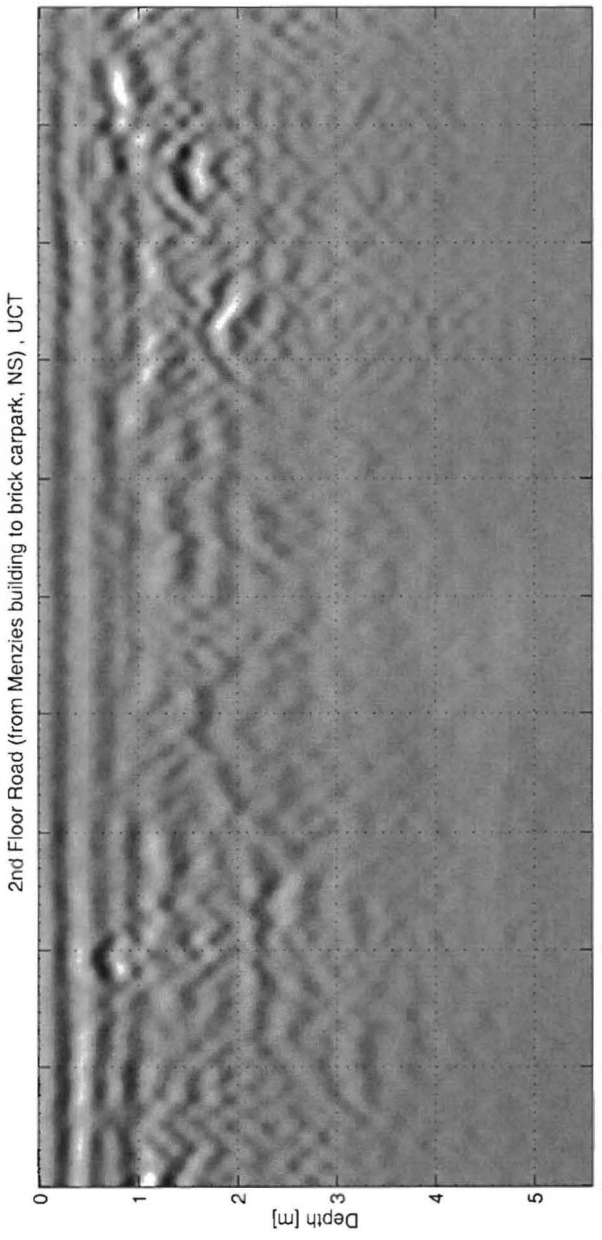

Figure E.1: Radar Measurement 1

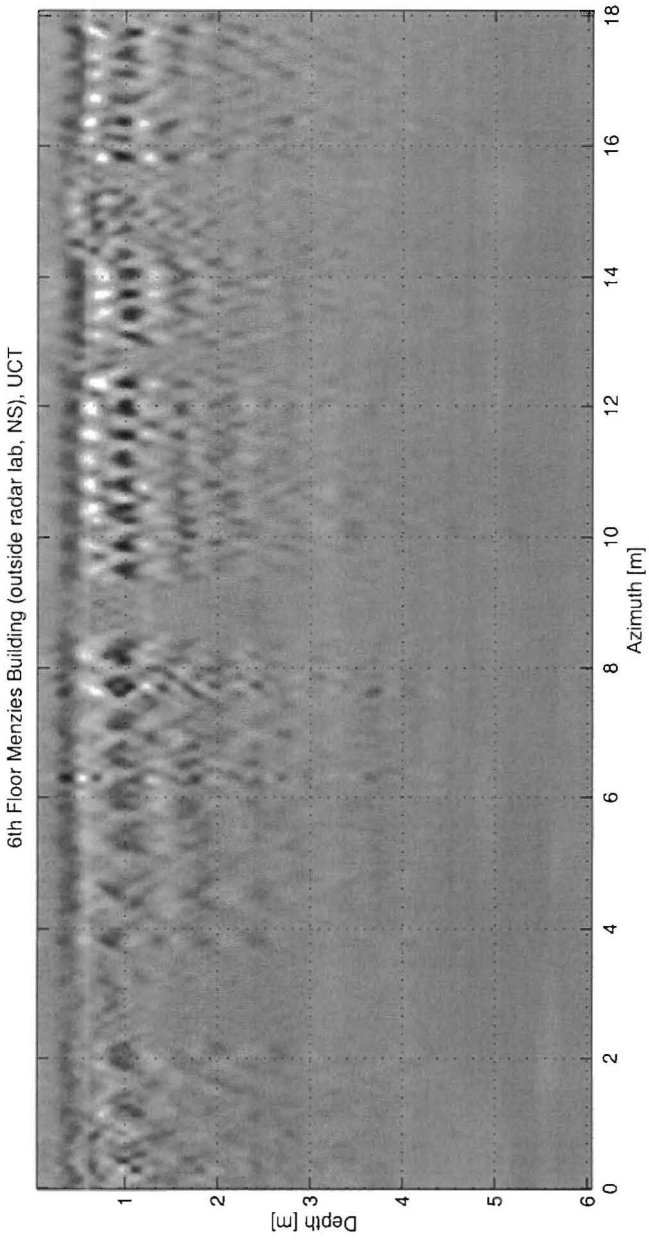

Figure E.2: Radar Measurement 2

Bibliography

[1] Anonymous. *Radio Frequency Oscillators and Synthesizers*, chapter 10, pages 10.9 10.24.

[2] E. J. Baghdady, R. N. Lincoln, and B. D. Nelin. Short-Term Frequency Stability: Characterization, Theory, and Measurement. *Proceedings of the IEEE*, pages 704 722, July 1965.

[3] Constantine A. Balanis. *Antenna Theory*. John Wiley & Sons, 1982.

[4] Cynthia L. Barker. Introduction to Single Chip Microwave PLLs. Technical Report AN-885, National Semiconductor, March 1993.

[5] James A. Barnes and et al. Characterization of Frequency Stability. *Transactions on Instrumentation and Measurement*, IM-20(2):105-120, May 1971.

[6] Jan Crols and Michael S. J. Steyaert. Low-IF Topologies for High-Performance Analog Front Ends of Fully Integrated Receivers. *IEEE Transactions on Circuits and Systems-II: Analog and Digital Signal Processing*, 45(3):269-282, March 1998.

[7] D.J. Daniels, D.J. Gunton, and H.F. Scott. Introduction to Sub-surface Radar. *IEE Proceedings Part F*, 135(4):277-320, August 1988.

[8] Jeffrey J. Daniels and James Brower. Side Looking Underground Radar (SLUR): Physical Modeling and Case History. *Geophysics*, 63(6):1-8, November 1998.

[9] Eduard A. Gerber and Arthur Ballato, editors. *Precision Frequency Control*. volume Volume 2, Oscillators and Standards. Academic Press, Inc., 1985.

[10] S.-E. Hamran, D.T. Gjessing, J. Hjelmstad, and E. Aarholt. Ground Penetrating Synthetic Pulse Radar: Dynamic Range and Modes of Operation. *Journal of Applied Geophysics*, 33(1-3):7-14, January 1995.

[11] K. C. Ho, Y. T. Chan, and R. Inkol. A Digital Quadrature Demodulation System. *IEEE Transactions on Aerospace and Electronic Systems*, 32(4):1218 1227, October 1996.

[12] S.A. Hovanessian. *Radar System Design and Analysis*. Artech House, Inc., 1984.

[13] Keigo Iizuka and Alois P. Freundorfer. Detection of Nonmetallic Buried Objects by a Step Frequency Radar. *Proceedings of the IEEE*, 71(2):276–279, February 1983.

[14] Keigo Iizuka, Alois P. Freundorfer, Kam Hung Wu, Hirotaka Mori, Hisanao Ogura, and Van-Khai Nguyen. Step-frequency radar. *J. Appl. Phys.*, 56(9):2572–2583, November 1984.

[15] Marten Kabutz. RF Hardware Design of a Stepped Frequency Continuous Wave Ground Penetrating Radar. Master's thesis, University of Cape Town, South Africa, June 1995.

[16] Alan Langman, Simon Dimaio, Brian Burns, and M.R. Inggs. Development of a Low Cost SFCW Ground Penetrating Radar. In *Proceedings of the IEEE 1996 Geoscience and Remote Sensing Symposium*, volume IV, pages 2020–2022, May 1996.

[17] Alan Langman and M. R. Inggs. New Technology UWB Stepped CW Radar. In *Proceedings of the PIERS workshop on Advances in Radar Methods*, volume ISBN 92-828-1947-7, July 1998.

[18] Hulin Liu, Arif Ghafoor, and Peter H. Stockman. A new quadrature sampling and processing approach. *IEEE Transactions on Aerospace and Electronic Systems*, 25(5):733 747, September 1989.

[19] Vadim Manassewitsch. *Frequency Synthesizers : Theory and Design*. John Wiley and Sons, 1976.

[20] David A. Noon and Glen F. Stickley. Antenna Ring-Down, Range-Sidelobes and Quality Factors of Time-and Frequency-Domain GPR Systems. In *Proceedings of the 7th International Conference on Ground Penetrating Radar (GPR'98)*, pages 63 68, Lawrence, Kansas, USA, May 27-30 1998.

[21] David Andrew Noon. *Stepped Frequency Radar Design and Signal Processing Enhances Ground Penetrating Radar Performance*. PhD thesis, University of Queensland, January 1996.

[22] Gary R. Olhoeft. `http://www.g-p-r.com/introduc.htm`.

[23] L. Peters, Jeffrey J. Daniels, and J. Young. Ground Penetrating Radar as a Subsurface Environmental Sensing Tool. *Proceedings of the IEEE*, 82(12):1802–1822, December 1994.

[24] Andrzej B. Przedpelski. Analyze, don't estimate, phase-lock-loop. *Electronic Design*, 26(10), May 1978.

[25] Andrzej B. Przedpelski. Optimize phase-lock loops to meet your needs-or determine why you can't. *Electronic Design*, 26(19), September 1978.

[26] Andrzej B. Przedpelski. Suppress phase-lock-loop sidebands without introducing instability. *Electronic Design*, 27(19), September 1979.

[27] Andrzej B. Przedpelski. Programmable calculator computes PLL noise, stability. *Electronic Design*, 29(7), March 1981.

[28] D. W. Rice and K. H. Wu. Quadrature Sampling with High Dynamic Range. *IEEE Transactions on Aerospace and Electronic Systems*, AES-18(4):736–739, November 1982.

[29] Jacques Rutman. Characterisation of Phase and Frequency Instabilites in Precision Frequency Sources: Fifteen Years of Progress. *Proceedings of the IEEE*, 66(9):1048–1075, September 1978.

[30] James A. Scheer and James L. Kurtz, editors. *Coherent Radar Performance Estimation*. Artech House, Inc., 685 Canton Street, Norwwod, MA 02062, 1993.

[31] A. Snip, I.L. Morrow, and P. van Genderen. Evaluation of Antennas in a Stepped Frequency Ground-Penetrating Radar for Location of Buried Objects. In *Proceedings Radar99*, Brest, France, 1999.

[32] Dr. William J. Steinway, Dr. Mark D. Patz, Peter L. Stern, Carrie J. Maggio, and James E. Thomas. An Improved Earth Penetration Radar Imaging System (EPRIS). In *Proceedings of the 7th International Conference on Ground Penetrating Radar (GPR'98)*, Lawrence, Kansas, USA, May 27–30 1998.

[33] Ronald C. Stirling. *Microwave Frequency Synthesizers*. Prentice-Hall, Inc., Englewood Cliffs, New Jersey 07632, 1987.

[34] David F. Stout. *Handbook of Operational Amplifier Circuit Designs*. McGraw-Hill, 1976.

[35] H. R. Ward. An optimum filter for direct A/D conversion. *IEEE Transactions on Aerospace and Electronic Systems*, 27(6):884–886, November 1991.

[36] W. M. Waters and B. R. Jarrett. Bandpass Signal and Coherent Detection. *IEEE Transactions on Aerospace and Electronic Systems*, AES-18(4):731–736, November 1982.

[37] Donald R. Wehner. *High-Resolution Radar*. Artech House, Inc., 685 Canton Street, Norwood, MA 02062, second edition edition, 1995.

[38] Yuanbin Wu and Jinwen Li. The design of digital radar receivers. In *Radar Conference, 1997, IEEE National*, pages 207–210, May 13–15 1997.

[39] Sun Xiaobing and Bao Zheng. Analysis and Experimental Results of Digital Quadrature Coherent Detector. In *Radar, 1996. Proceedings., CIE International Conference of*, pages 381–384. IEEE, October 8–10 1996.